Journal of Ocean Engineering and Science 9 (2024) 461–474

Contents lists available at ScienceDirect

Journal of Ocean Engineering and Science

journal homepage: www.elsevier.com/locate/joes

Analysis of travelling wave solutions of double dispersive sharma-Tasso-Olver equation☆

Kamruzzaman Khan[a,e,*], Henk Koppelaar[b], M. Ali Akbar[c], Syed Tauseef Mohyud-Din[d]

[a] Department of Mathematics, Pabna University of Science and Technology, Pabna 6600, Bangladesh
[b] Fac. of Electrical Eng., Mathematics and Comp. Science, University of Delft, Netherlands
[c] Department of Applied Mathematics, University of Rajshahi, Rajshahi 6205, Bangladesh
[d] Department of Mathematics, HITEC University Taxila Cantt, Pakistan
[e] School of Science and Technology, University of New England, Armidale, NSW 2351, Australia

ARTICLE INFO

Article history:
Received 27 November 2021
Revised 28 February 2022
Accepted 18 March 2022
Available online 23 March 2022

Keywords:
Travelling wave
Solitary wave
Streamline
Enhanced (G'/G)-expansion method
STO equation

ABSTRACT

Travelling wave solutions have been played a vital role in demonstrating the wave character of nonlinear problems arising in the field of ocean engineering and sciences. To describe the propagation of the nonlinear wave phenomenon in the ocean (for example, wind waves, tsunami waves), a variety of evolution equations have been suggested and investigated in the existing literature. This paper studies the dynamic of travelling periodic and solitary wave behavior of a double–dispersive non-linear evolution equation, named the Sharma-Tasso-Olver (STO) equation. Nonlinear evolution equations with double dispersion enable us to describe nonlinear wave propagation in the ocean, hyperplastic rods and other mediums in the field of science and engineering. We analyze the wave solutions of this model using a combination of numerical simulations and Ansatz techniques. Our analysis shows that the travelling wave solutions involve a range of parameters that displays important and very interesting properties of the wave phenomena. The relevance of the parameters in the travelling wave solutions is also discussed. By simulating numerically, we demonstrate how parameters in the solutions influence the phase speed as well as the travelling and solitary waves. Furthermore, we discuss instantaneous streamline patterns among the obtained solutions to explore the local direction of the components of the obtained solitary wave solutions at each point in the coordinate (x, t).

1. Introduction

Nonlinear evolution equations are widely used to model Ocean and atmospheric dynamics [61–65]. Ocean engineering is concerned with large scale wave motions in the ocean (for example, wind waves, tsunami waves) and air along with the temperature and density of water in the ocean. Ocean and atmosphere are equally important in carrying energy from one place to another in the form of wave propagation. Despite published Sharma-Tasso-Olver (STO) soliton solutions (before December 2020: [1–12]), we find new solutions of this type of nonlinear evolution equations (NLEEs). The STO nonlinear equation is $u_t + \alpha(u^3)_x + \frac{3}{2}\alpha\,(u^2)_{xx} + \alpha\,u_{xxx} = 0$ and belongs to the Burgers equation hierarchy with $n = 2$:

$$u_t + \alpha\frac{\delta}{\delta x}\left(\frac{\delta}{\delta x} + u\right)^n u = 0, \quad n = 0, 1, 2, \ldots \tag{0.1}$$

The second and third derivative terms are known as the first and second-order dispersion, respectively [43]. Nonlinear evolution equations with double dispersion enable us to describe nonlinear wave propagation in the ocean, hyperplastic rod (for instance, Murnaghan rod) [44], and other fields of science and engineering. The key feature of the STO equation is the presence of two sources of dispersion (first and second-order dispersion), characterized by the terms u_{xx} and u_{xxx}. When the exchange of energy between the surface of nonlinear media and the medium of wave propagation is considered, double dispersion can occur.

Our method to get new solutions is the enhanced (G'/G)-expansion method, co-designed by two of us (K.K and A.MA) [13-16, 60], though Naher [17] refers to only one of us. Kudryashov [18] observed that new solutions were often announced because a

☆ Mathematics Subject Classification: 20.11, 40.03, 40.09, 40.11, 40.12, 40.17

* Corresponding author.
E-mail address: k.khanru@gmail.com (K. Khan).

https://doi.org/10.1016/j.joes.2022.03.018

new method produces a seemingly new solution by lack of simplification. After simplification of its results, the method appears to be equivalent to some of the other methods. Most of the methods output tanh solutions of the STO equation, even for the fractional STO.

In 1977 Sharma and Tasso [19] published an equation in the same year with Olver's paper [20] which in 1982 became known as the Sharma-Tasso-Olver (STO) equation [21]. Many papers became published, including solutions of the fractional derivative STO equation [22, 23], fusion/fission STO [2,5,6], STO-like new types of equations [22]. By the introduction of an imaginary coefficient Fan [24, 25] derived a complex STO equation, cSTO for short, in [5]. The relation between cSTO and the Kaup-Newell hierarchy is observed in [26], while integrable combined STO and Burgers equations are treated by Zhao [27].

The very first exact solutions of the STO equation by Hereman et al. [1] are of the tanh type, also chosen two years later by Kudryashov [28] among his 'Ansatze'. Among the solution methods for NLEEs that have been developed, are Hirota's Method [6], the Inverse Scattering Transform [29], Fan's Auto-Bäcklund Method [30], the Cole-Hopf transformation for linearization [31], the Homotopy Perturbation Method (finds STO solutions in the tanh format) [32], Group Invariants, Symmetry solutions, conservation laws [7, 33], the Exp-function method [34], the q-homotopy analysis transform method [45], the improved Sardar sub-equation method [46], the auxiliary equation method [47, 48], the Jacobi elliptic functions [49], the Bernoulli sub-ODE [50], the meshless collocation method [51], the generalized exponential rational function method [52], trial function method [53], the generalized logistic equation method [54], the nonlocal integrable reduction [55, 56], the nonlocal group reduction [57], An innovative algorithm to verify the Hirota N-soliton condition [58,59], the modified F-expansion [61] to name a few.

The purpose of this paper is to study the relevance of the parameters in the travelling periodic and solitary wave solutions to demonstrate how parameters in the solutions influence the phase speed as well as the travelling and solitary waves. Furthermore, we discuss instantaneous streamline patterns among the obtained solutions to explore the local direction of the components of the solitary wave solutions at each point in the coordinate (x, t).

The rest of the paper is organised as follows. In Section 2, we repeat the steps from our algorithm [15] to simplify references to the applications in Section 3. In Section 3, the enhanced (G'/G)-expansion method is applied to the STO equation to find travelling periodic and solitary wave solutions. In Section 4, the analysis and physical structure of the results are presented. In Section 5, Streamlines among the obtained solutions are investigated. In Section 6, we examine the phase speed and the pattern of the obtained solutions numerically to gain a better understanding of the effect of parameters. In Section 7, Conclusions are given.

2. Description of the enhanced (G'/G)-expansion method

In this section, we repeat the steps of the Enhanced (G'/G)-Expansion Method for finding travelling wave solutions of NLEEs. Suppose that a NLEE, say in two independent variables x and t is given by

$$\Re(u,\ u_t,\ u_x, u_{tt},\ u_{xx},\ u_{xt},\ \cdots) = 0, \tag{2.1}$$

where $u(\xi) = u(x,t)$ is an unknown function, $\Re$ is a polynomial of $u(x,t)$and its partial derivatives in which the highest order derivatives and nonlinear terms are involved. Below, we give the main steps of this applied expansion method:

Step 1. Combining the independent variables x and t into one variable $\xi = x \pm \omega t$, we suppose that

$$u(\xi) = u(x,t), \quad \xi = x \pm \omega t, \tag{2.2}$$

In Cartesian coordinates with x horizontal and ξ vertical, $\xi = \xi(x,t)$ specifies the waveform where ω is the phase speed, and $\xi = x \pm \omega\ t$ is the phase.

The travelling wave transformation Eq. (2.2) permits us to reduce Eq. (2.1) to the following ODE:

$$\Re(u,\ u',\ u'',\ \cdots\cdots) = 0, \tag{2.3}$$

where $\Re$ is a polynomial in $u(\xi)$ with its derivatives $u'(\xi) = \frac{du}{d\xi}$, $u''(\xi) = \frac{d^2u}{d\xi^2}$ and so on.

Step 2. We suppose that Eq. (2.3) has a formal solution of the following format

$$u(\xi) = \sum_{i=-n}^{n} \left(\frac{a_i(\psi(\xi))^i}{(1+\lambda\,\psi(\xi))^i} + b_i(\psi(\xi))^{i-1} \sqrt{\sigma\left(1 + \frac{1}{\mu}(\psi(\xi))^2\right)} \right), \tag{2.4}$$

where $\psi(\xi) = \frac{G'}{G}$, and $G = G(\xi)$ satisfies the equation

$$G'' + \mu G = 0, \tag{2.5}$$

with constants $a_i,\ b_i\ (-n \le i \le n;\ n \in \mathrm{N})$ and λ to be determined later, and $\sigma = \pm 1,\ \mu \ne 0$.

Step 3. The positive integer n can be determined by considering the homogeneous balance between the highest order derivatives and the nonlinear terms appearing in Eq. (2.1) or Eq. (2.3). Moreover precisely, we define the degree of $u(\xi)$ as $D(u(\xi)) = n$ which enables us to find the degree of other expressions as follows

$$D\left(\frac{d^q u}{d\xi^q}\right) = n + q,\ D\left(u^p \left(\frac{d^q u}{d\xi^q}\right)^s\right) = np + s(n+q). \tag{2.6}$$

Therefore, we can find the value of nnin Eq. (2.4), using Eq. (2.6).

Step 4. We substitute Eq. (2.4) into Eq. (2.3) using Eq. (2.5), then collect all terms of the same powers of $(\psi(\xi))^j$ and $(\psi(\xi))^j\sqrt{\sigma\,(1+\frac{1}{\mu}(\psi(\xi))^2)}$ together. We then set each coefficient to zero to obtain an over-determined system of algebraic equations and solve this system for a_i, b_i, λ and ω.

Step 5. From the general solution of Eq. (2.5), we get

When $\mu < 0$,

$$\psi(\xi) = \sqrt{-\mu}\tanh\left(A + \sqrt{-\mu}\xi\right) \tag{2.7}$$

And

$$\psi(\xi) = \sqrt{-\mu}\coth\left(A + \sqrt{-\mu}\xi\right) \tag{2.8}$$

Again, when $\mu > 0$,

$$\psi(\xi) = \sqrt{\mu}\tan\left(A - \sqrt{\mu}\xi\right) \tag{2.9}$$

And

$$\psi(\xi) = \sqrt{\mu}\cot\left(A + \sqrt{\mu}\xi\right) \tag{2.10}$$

where A is an arbitrary constant. Finally, substituting $a_i,\ b_i\ (-n \le i \le n;\ n \in \mathrm{N})$, λ, ω and Eqs. (2.7) - (2.10) into Eq. (2.4) we obtain travelling wave solutions of Eq. (2.1).

3. Sharma-Tasso-Olver equation

In this section, we will exert the enhanced (G'/G)-expansion method to solve the STO equation in the format derived from Burgers' equation with $n = 2$

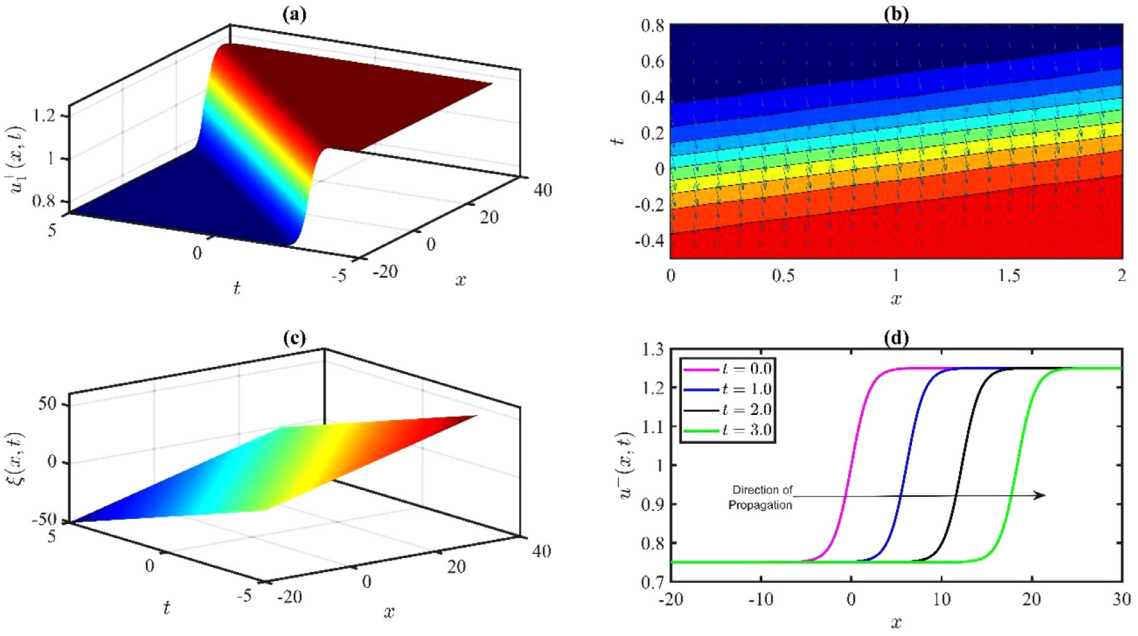

Fig. 1. Profile of $u_1^+(x,t)$, which is moving in the positive direction of the x-axis with the phase speed $\omega = {}^{-6.125}$ [1]. Figure (a) represents the 3D profile of $u_1^+(x,t)$ for the *real part* with the values of $\mu = -0.25,\ A = 0,\ a_0 = 1,\ \alpha = 1$. Figure (b) represents the corresponding contour plot of (a) along with arrows of the directional components at the point (x,t). Figure (c) is the corresponding profile of *phase* $\xi(x,t) = x + \omega t$. Figure (d) indicates the progress of the travelling wave as time increases, where snapshots are taken at time $t = 0,\ 1,\ 2,\ 3$. Figure (d) represents the time evolution of the solution u_1^+, which suggests that the solitary wave is propagating in the positive direction of the x-axis.

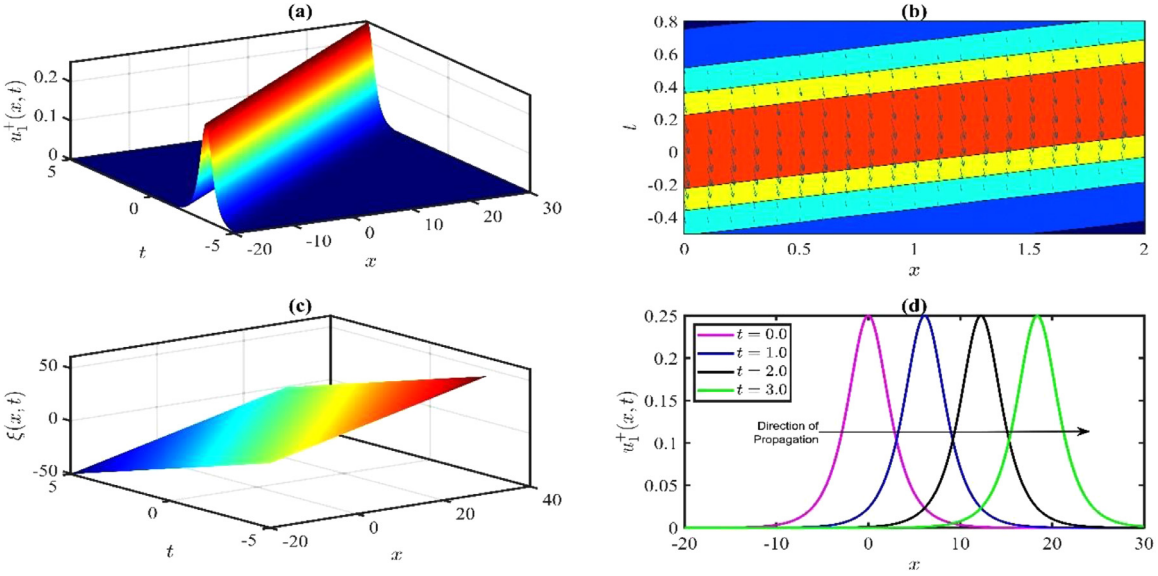

Fig. 2. Profile of $u_1^+(x,t)$, which is moving in the positive direction of the x-axis with the phase speed $\omega = -6.125$. Figure (a) represents the 3D profile of $u_1^+(x,t)$ for the *imaginary part* with the values of $\mu = -0.25,\ A = 0,\ a_0 = 1,\ \alpha = 1$. Figure (b) represents the corresponding contour plot of (a) along with arrows of the directional components of instantaneous streamline. Figure (c) is the corresponding profile of wave phase $\xi(x,t) = x + \omega t$. Figure (d) indicates the progress of the travelling wave as time increases, where snapshots are taken at time $t = 0,\ 1,\ 2,\ 3$. Figure (d) represents the time evolution of the solution u_1^+, which suggests that the solitary wave is propagating in the positive direction of the x-axis.

$$u_t + \alpha\left(u^3\right)_x + \frac{3}{2}\alpha\left(u^2\right)_{xx} + \alpha\, u_{xxx} = 0, \tag{3.1}$$

where $u(x,t)$ is the amplitude of the relative wave mode and $\alpha$is a nonzero constant.

The travelling wave transformation equation $u(x,t) = u(\xi)$, $\xi = x + \omega t$ transforms Eq. (3.1) to the ordinary differential equation

$$\omega u' + \alpha(u^3)' + \frac{3}{2}\alpha(u^2)'' + \alpha u''' = 0. \tag{3.2}$$

Now integrating Eq. (3.2) with respect to ξ once , we have

$$\alpha u'' + 3\alpha u u' + \omega u + \alpha u^3 + R = 0, \tag{3.3}$$

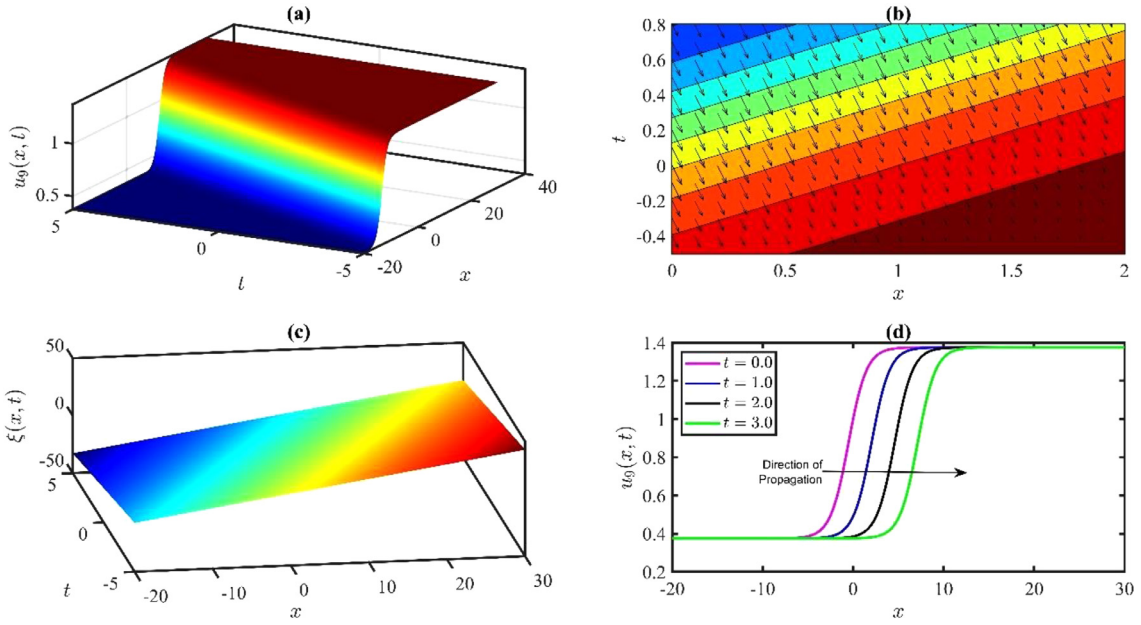

Fig. 3. Profile of $u_9(x,t)$, which is moving in the positive direction of the x-axis with the phase speed $\omega = -2.5468$. Figure (a) represents the 3D profile of $u_9(x,t)$ for the values of $\mu = -0.25,\ A = 0,\ a_0 = 1,\ \alpha = 1,\ \lambda = 0.5$. Figure (b) represents the corresponding contour plot of (a) along with arrows of the directional components. Figure (c) is the corresponding profile of wave phase $\xi(x,t) = x + \omega t$. Figure (d) indicates the progress of the travelling wave as time increases, where snapshots are taken at time $t = 0,\ 1,\ 2,\ 3$. Figure (d) represents the time evolution of the solution u_9, which suggests that the solitary wave is propagating in the positive direction of the x-axis.

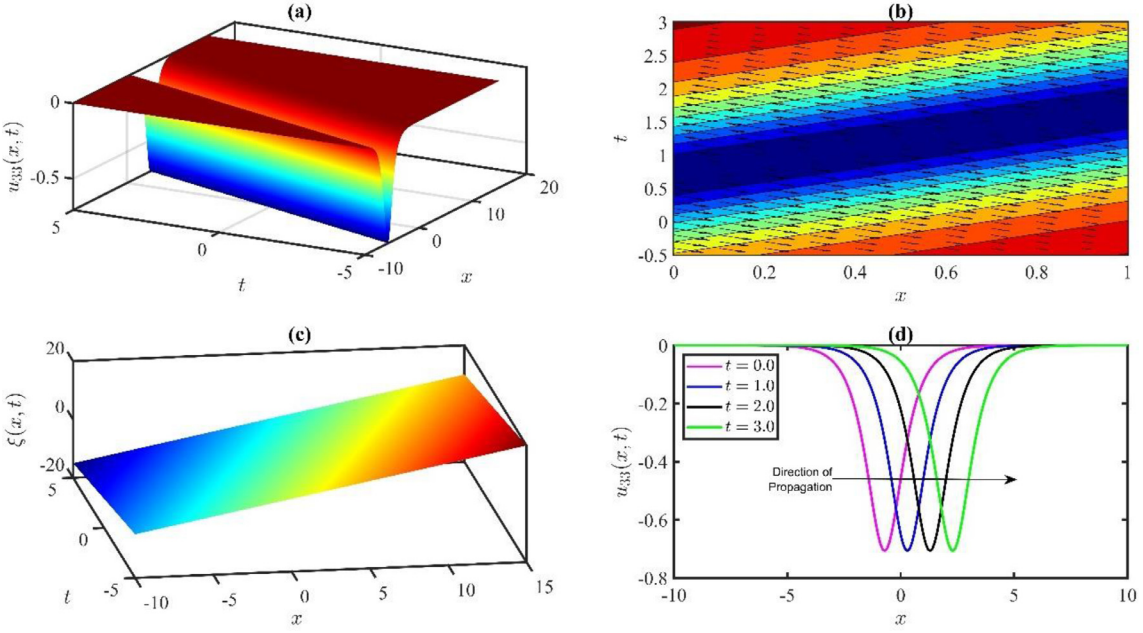

Fig. 4. Profile of $u_{33}(x,t)$, which is moving in the positive direction of the x-axis with the phase speed $\omega = -1$. Figure (a) represents the 3D profile of $u_{33}(x,t)$ for the *real part* with the values of $\mu = -2,\ A = 1,\ a_0 = 0,\ \alpha = 0.5,\ \lambda = 0$. Figure (b) represents the corresponding contour plot of (a) along with arrows of the directional components. Figure (c) is the corresponding profile of wave phase $\xi(x,t) = x + \omega t$. Figure (d) indicates the progress of the travelling wave as time increases, where snapshots are taken at time $t = 0,\ 1,\ 2,\ 3$. Figure (d) represents the time evolution of the solution u_{33} which suggests that the solitary wave is propagating in the positive direction of the x-axis.

where R is a constant of integration. Balancing the highest-order derivative term u'' and the nonlinear term u^3 from Eq. (3.3), yields $n = 1$. Hence for $n = 1$ Eq. (2.4) reduces to

$$u(\xi) = \frac{a_{-1}(1+\lambda\,\psi(\xi))}{\psi(\xi)} + a_0 + \frac{a_1\,\psi(\xi)}{1+\lambda\,\psi(\xi)} + b_{-1}(\psi(\xi))^{-2}\sqrt{\sigma\left(1+\frac{1}{\mu}(\psi(\xi))^2\right)} + b_0(\psi(\xi))^{-1}\sqrt{\sigma\left(1+\frac{1}{\mu}(\psi(\xi))^2\right)} + b_1\sqrt{\sigma\left(1+\frac{1}{\mu}(\psi(\xi))^2\right)}, \tag{3.4}$$

where $G = G(\xi)$ satisfies Eq. (2.5). Substitute Eq. (3.4) along with Eq. (2.5) into Eq. (3.3). As a result of this substitution, we get a polynomial of $(\psi(\xi))^j$ and $(\psi(\xi))^j\sqrt{\sigma(1+\frac{1}{\mu}(\psi(\xi))^2)}$. From these polynomials, we equate the coefficients of $(\psi(\xi))^j$ and

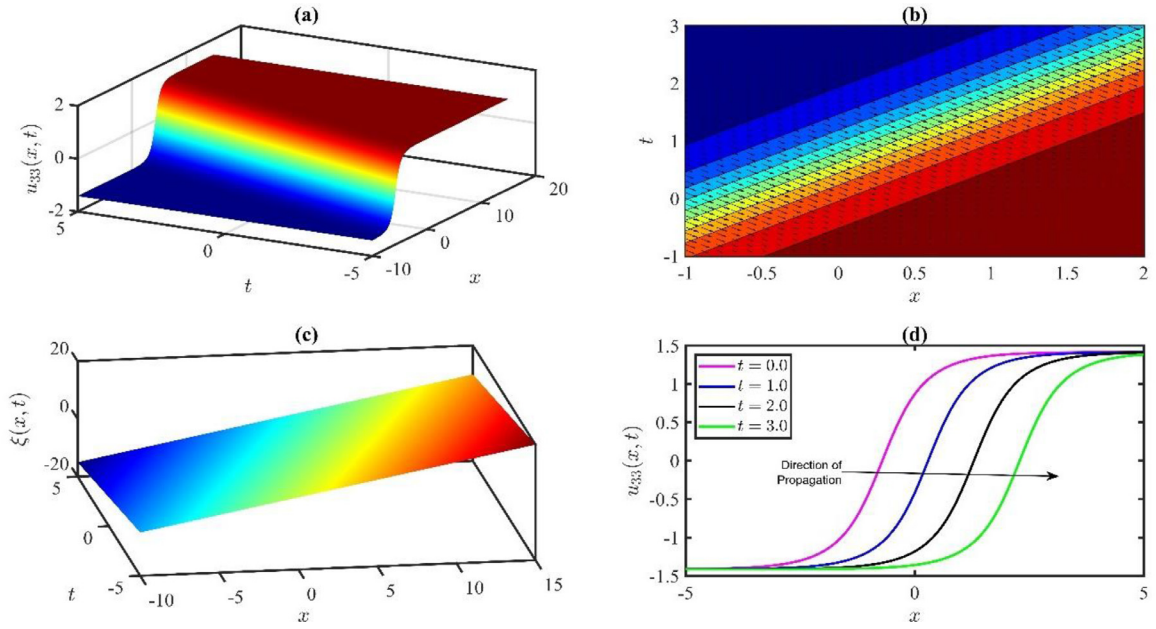

Fig. 5. Profile of $u_{33}(x,t)$, which is moving in the positive direction of the x-axis with the phase speed $\omega = -1$. Figure (a) represents the 3D profile of $u_{33}(x,t)$ for the *imaginary part* with the values of $\mu = -2,\ A = 1,\ a_0 = 0,\ \alpha = 0.5,\ \lambda = 0$. Figure (b) represents the corresponding contour plot of (a) along with arrows of the directional components. Figure (c) is the corresponding profile of wave phase $\xi(x,t) = x + \omega t$. Figure (d) indicates the progress of the travelling wave as time increases, where snapshots are taken at time $t = 0,\ 1,\ 2,\ 3$. Figure (d) represents the time evolution of the solution u_{33}, which suggests that the solitary wave is propagating in the positive direction of the x-axis.

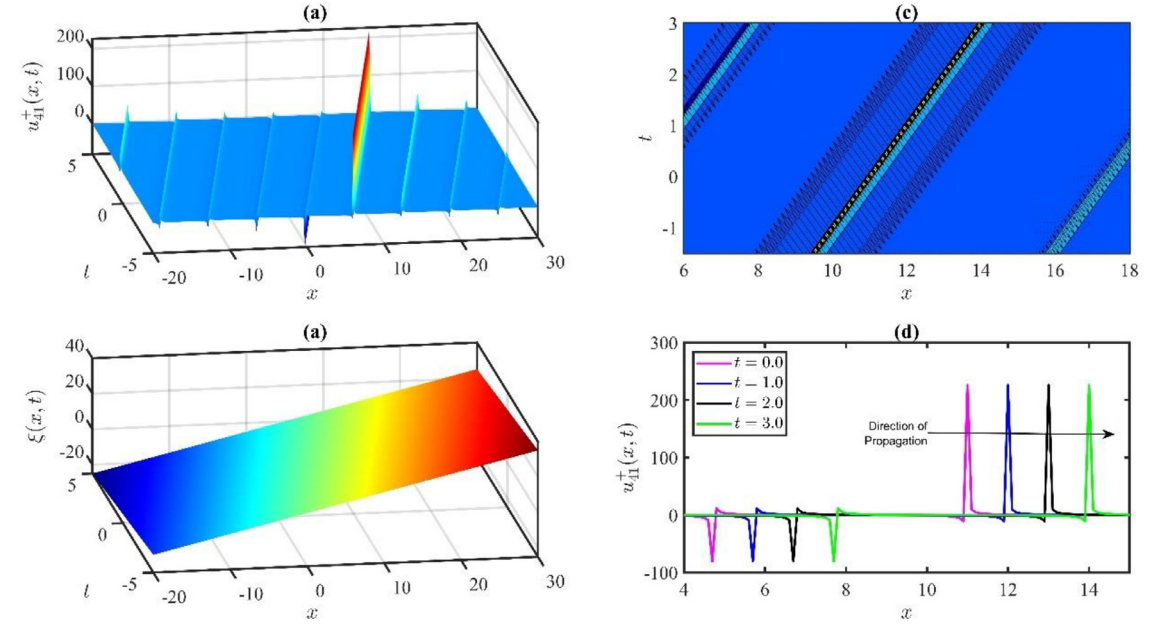

Fig. 6. Profile of $u_{41}(x,t)$, which is moving in the positive direction of the x-axis with the phase speed $\omega = -1$. Figure (a) represents the 3D profile of $u_{41}(x,t)$ for the values of $\mu = 1,\ A = 0,\ a_0 = 0,\ \alpha = -2$. Figure (b) represents the corresponding contour plot of (a) along with arrows of the directional components. Figure (c) is the corresponding profile of wave phase $\xi(x,t) = x + \omega t$. Figure (d) indicates the progress of the travelling wave as time increases, where snapshots are taken at time $t = 0,\ 1,\ 2,\ 3$. Figure (d) represents the time evolution of the solution u_{41}, which suggests that the solitary wave is propagating in the positive direction of the x-axis.

$(\psi(\xi))^j \sqrt{\sigma(1 + \frac{1}{\mu}(\psi(\xi))^2)}$, and setting them to zero, we get an over-determined system consisting of twenty-five algebraic equations. Solving this system for a_i, b_i, λ and ω we obtain the following fourteen sets of values with the aid of the symbolic computer software Maple.

Set 1: $R = \frac{1}{2}\alpha a_0(\mu + 4{a_0}^2),\ \omega = \frac{1}{2}\alpha(\mu - 12{a_0}^2),\ \lambda = 0,\ a_{-1} = 0,\ a_0 = a_0,\ a_1 = \frac{1}{2},\ b_{-1} = b_0 = b_1 = 0.$

Set 2: $R = 0,\ \omega = \alpha\mu,\ \lambda = 0,\ a_{-1} = 0,\ a_0 = 0,\ a_1 = 1,\ b_{-1} = b_0 = 0,\ b_1 = \pm\sqrt{\frac{\mu}{\sigma}}.$

Set 3: $R = 2\alpha({a_0}^3 + 3a_0\mu^2\lambda^2 + a_0\mu + 3{a_0}^2\mu\lambda + \mu^3\lambda^3 + \mu^2\lambda),\ \lambda = \lambda,\ a_{-1} = 0,\ a_0 = a_0,$
$a_1 = \mu\lambda^2 + 1,\ \omega = -3{a_0}^2\alpha - 3\alpha\mu^2\lambda^2 + \alpha\mu - 6\alpha a_0\mu\lambda,\ b_{-1} = b_0 = b_1 = 0.$

Set 4: $R = 0,\ \omega = 4\alpha\mu,\ \lambda = \lambda,\ a_{-1} = 0,\ a_0 = -2\mu\lambda,\ a_1 = 2\mu\lambda^2 + 2,\ b_{-1} = b_0 = b_1 = 0.$

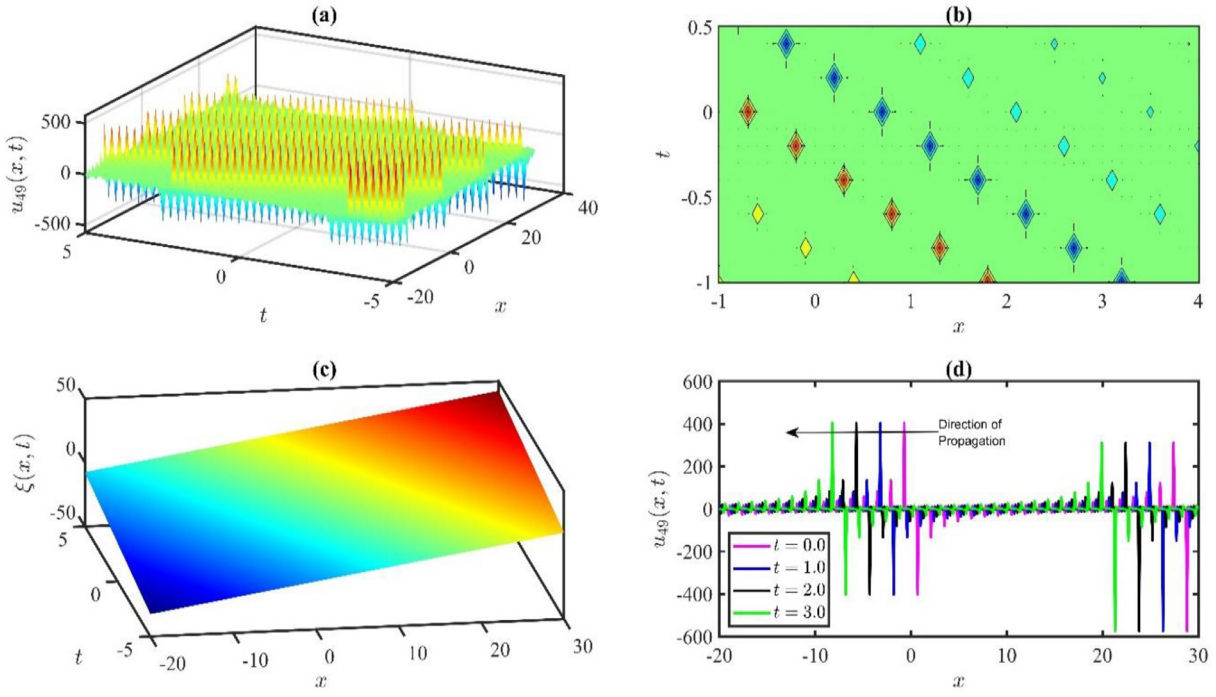

Fig. 7. Profile of $u_{49}(x,t)$, which is moving in the negative direction of the x-axis with the phase speed $\omega = 2.5$. Figure (a) represents the 3D profile of $u_{49}(x,t)$ for the values of $\mu = 5,\ A = 0,\ a_0 = 0,\ \alpha = 0.5,\ \lambda = 0$. Figure (b) represents the corresponding contour plot of (a) along with arrows of the directional components. Figure (c) is the corresponding profile of wave phase $\xi(x,t) = x + \omega t$. Figure (d) indicates the progress of the travelling wave as time increases, where snapshots are taken at time $t = 0,\ 1,\ 2,\ 3$. Figure (d) represents the time evolution of the solution u_{49}, which suggests that the solitary wave is propagating in the negative direction of the x-axis.

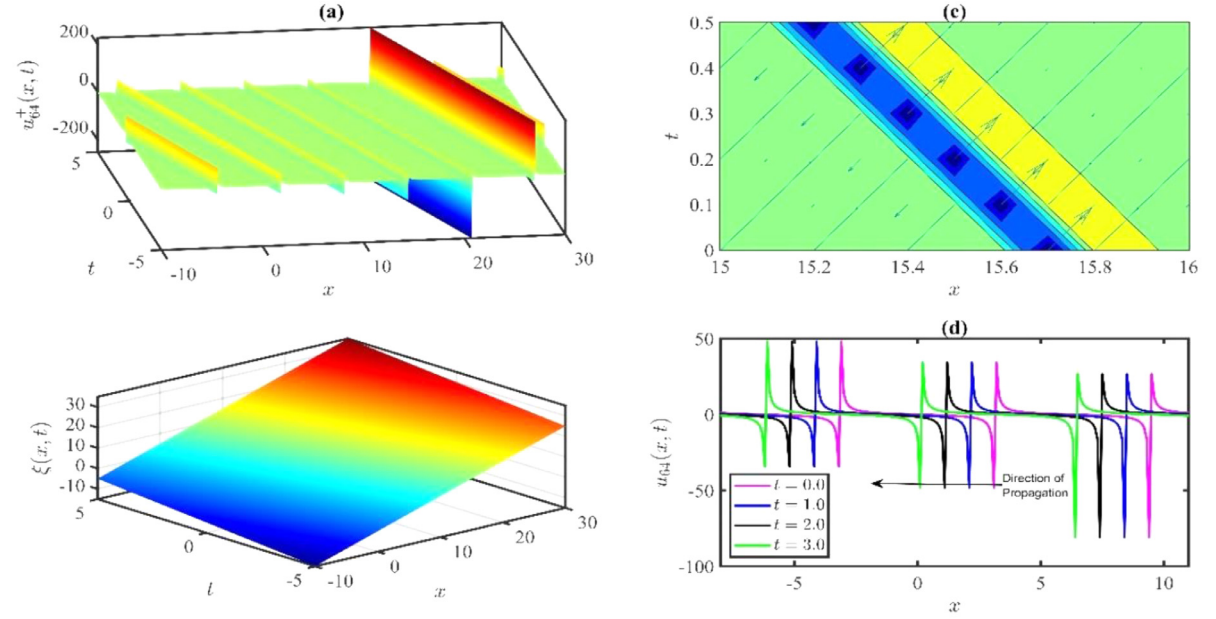

Fig. 8. Profile of $u_{64}(x,t)$, which is moving in the negative direction of the x-axis with the phase speed $\omega = 1$. Figure (a) represents the 3D profile of $u_{64}(x,t)$ for the values of $\mu = 0.25,\ A = 0,\ a_0 = 1,\ \alpha = 1$. Figure (b) represents the corresponding contour plot of (a) along with arrows of the directional components. Figure (c) is the corresponding profile of wave phase $\xi(x,t) = x + \omega t$. Figure (d) indicates the progress of the travelling wave as time increases, where snapshots are taken at time $t = 0,\ 1,\ 2,\ 3$. Figure (d) represents the time evolution of the solution u_{64}, which suggests that the solitary wave is propagating in the negative direction of the x-axis.

Set 5: $R = 0,\ \omega = 4\alpha\mu,\ \lambda = \lambda,\ a_{-1} = -\mu,\ a_0 = 0,\ a_1 = \mu\lambda^2 + 1,\ b_{-1} = b_0 = b_1 = 0.$

Set 6: $R = -2\alpha(-{a_0}^3 - 3a_0\mu^2\lambda^2 - a_0\mu + 3{a_0}^2\mu\lambda + \mu^3\lambda^3 + \mu^2\lambda),\ \lambda = \lambda,\ a_{-1} = -\mu,\ a_0 = a_0,$
$a_1 = 0,\ \omega = -3{a_0}^2\alpha - 3\alpha\mu^2\lambda^2 + \alpha\mu + 6\alpha a_0\mu\lambda,\ b_{-1} = b_0 = b_1 = 0.$

Set 7: $R = 2a_0\alpha(4\mu + {a_0}^2),\ \omega = 4\alpha\mu - 3{a_0}^2\alpha,\ \lambda = 0,\ a_{-1} = -\mu,\ a_0 = a_0,\ a_1 = 1,\ b_{-1} = b_0 = b_1 = 0.$

Set 8: $R = \pm\frac{160}{27}\frac{\alpha\mu^2}{\sqrt{-\mu}},\ \omega = \frac{28}{3}\alpha\mu,\ \lambda = \mp\frac{1}{3\sqrt{-\mu}},\ a_{-1} = -\mu,\ a_0 = \mp\frac{2}{3}\sqrt{-\mu},$
$a_1 = \frac{16}{9},\ b_{-1} = b_0 = b_1 = 0.$

Set 9: $R = 0,\ \omega = 4\alpha\mu,\ \lambda = \lambda,\ a_{-1} = -2\mu,\ a_0 = 2\mu\lambda,\ a_1 = 0,\ b_{-1} = b_0 = b_1 = 0.$

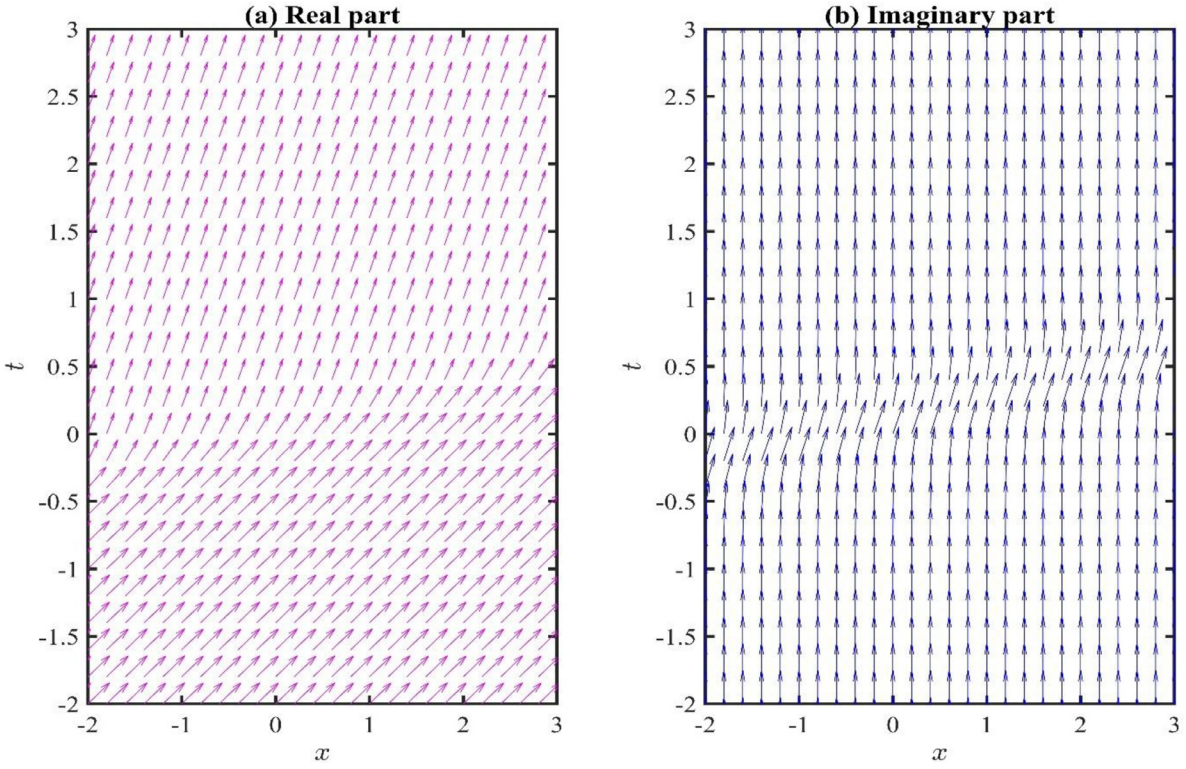

Fig. 9. Instantaneous streamline pattern between $u_1(x,t)$ and $u_9(x,t)$ for the values of $\mu=-1,\ A=0,\ a_0=1,\ \alpha=2,\ \lambda=1$. Arrows in figures (a) and (b) depicted the direction of wave components. In Figure (a) real part and Figure (b) imaginary part of $u_1(x,t)$ are used.

Set 10: $R=0,\ \omega=16\alpha\mu,\ \lambda=0,\ a_{-1}=-2\mu,\ a_0=0,\ a_1=2,\ b_{-1}=b_0=b_1=0.$

Set 11: $R=\mp\frac{160}{27}\frac{\alpha\mu^2}{\sqrt{-\mu}},\ \omega=\frac{28}{3}\alpha\mu,\ \lambda=\mp\frac{1}{3\sqrt{-\mu}},\ a_{-1}=-2\mu,\ a_0=\pm\frac{2}{3}\sqrt{-\mu},$
$a_1=\frac{8}{9},\ b_{-1}=b_0=b_1=0.$

Set 12: $R=0,\ \omega=\alpha\mu,\ \lambda=\lambda,\ a_{-1}=-\mu,\ a_0=\mu\lambda,\ a_1=0,\ b_{-1}=0,\ b_0=\pm\frac{\mu}{\sqrt{\sigma}},\ b_1=0.$

Set 13: $R=0,\ \omega=\alpha\mu,\ \lambda=0,\ a_{-1}=-\frac{\mu}{2},\ a_0=0,\ a_1=\frac{1}{2},\ b_{-1}=0,\ b_0=\pm\frac{\mu}{2\sqrt{\sigma}},\ b_1=\pm\frac{1}{2}\sqrt{\frac{\mu}{\sigma}}.$

Set 14: $R=-\frac{1}{4}\alpha(\mu^2\lambda-6a_0\mu^2\lambda^2+12a_0{}^2\mu\lambda+\mu^3\lambda^3-2a_0\mu-8a_0{}^3),\ \lambda=\lambda,\ a_{-1}=-\frac{\mu}{2},\ a_0=a_0,$
$a_1=0,\ \omega=-\frac{1}{4}\alpha(-\mu-12a_0\mu\lambda+12a_0{}^2+3\mu^2\lambda^2),\ b_{-1}=0,\ b_0=\frac{\mu}{2\sqrt{\sigma}},\ b_1=0.$

Hyperbolic function solutions ($\mu<0$): Substituting Eq. (2.7) and Eq. (2.8) into Eq. (3.4) along with Set 1- 14, we get respectively the families of hyperbolic function solutions mentioned below. If a family has been reported before its first reference in the literature list is mentioned.

Family 1: $u_{1,2}(\xi)=a_0+\frac{1}{2}\sqrt{-\mu}(\tanh(A+\sqrt{-\mu}\,\xi)\pm I\mathrm{sech}(A+\sqrt{-\mu}\,\xi)),\ u_{3,4}(\xi)=a_0+\frac{1}{2}\sqrt{-\mu}(\coth(A+\sqrt{-\mu}\,\xi)\mp\mathrm{csch}(A+\sqrt{-\mu}\,\xi))$, where $\xi=x+(\frac{1}{2}\alpha(\mu-12a_0{}^2))\,t$.

Family 2: $u_{5,6}(\xi)=\sqrt{-\mu}(\tanh(A+\sqrt{-\mu}\xi)\pm I\mathrm{sech}(A+\sqrt{-\mu}\xi)),\ u_{7,8}(\xi)=\sqrt{-\mu}(\coth(A+\sqrt{-\mu}\xi)\mp\mathrm{csch}(A+\sqrt{-\mu}\xi))$, where $\xi=x+\alpha\mu\,t$.

Family 3: $u_9(\xi)=a_0+\sqrt{-\mu}\,(1+\mu\,\lambda^2)(\frac{\tanh(A+\sqrt{-\mu}\xi)}{1+\lambda\sqrt{-\mu}\tanh(A+\sqrt{-\mu}\xi)}),\ u_{10}(\xi)=a_0+\sqrt{-\mu}\,(1+\mu\,\lambda^2)(\frac{\coth(A+\sqrt{-\mu}\xi)}{1+\lambda\sqrt{-\mu}\coth(A+\sqrt{-\mu}\xi)})$, where $\xi=x+(-3a_0{}^2\alpha-3\alpha\mu^2\lambda^2+\alpha\mu-6\alpha a_0\mu\lambda)\,t$. This Family has been obtained before [11].

Family 4: $u_{11}(\xi)=-2\mu\lambda+2\sqrt{-\mu}\,(1+\mu\,\lambda^2)(\frac{\tanh(A+\sqrt{-\mu}\xi)}{1+\lambda\sqrt{-\mu}\tanh(A+\sqrt{-\mu}\xi)}),\ u_{12}(\xi)=-2\mu\lambda+2\sqrt{-\mu}\,(1+\mu\,\lambda^2)(\frac{\coth(A+\sqrt{-\mu}\xi)}{1+\lambda\sqrt{-\mu}\coth(A+\sqrt{-\mu}\xi)})$, where $\xi=x+4\alpha\mu\,t$. This Family has been obtained before [11].

Family 5: $u_{13}(\xi)=\sqrt{-\mu}\,(\frac{(1+\mu\,\lambda^2)\tanh(A+\sqrt{-\mu}\xi)}{1+\lambda\sqrt{-\mu}\tanh(A+\sqrt{-\mu}\xi)}+\coth(A+\sqrt{-\mu}\xi)+\lambda\sqrt{-\mu}),\ u_{14}(\xi)=\sqrt{-\mu}\,(\frac{(1+\mu\,\lambda^2)\coth(A+\sqrt{-\mu}\xi)}{1+\lambda\sqrt{-\mu}\coth(A+\sqrt{-\mu}\xi)}+\tanh(A+\sqrt{-\mu}\xi)+\lambda\sqrt{-\mu})$, where$\xi=x+4\alpha\mu\,t$. This Family combines 4 and 6.

Family 6: $u_{15}(\xi)=a_0+\sqrt{-\mu}(\coth(A+\sqrt{-\mu}\xi)+\lambda\sqrt{-\mu})$,
$u_{16}(\xi)=a_0+\sqrt{-\mu}(\tanh(A+\sqrt{-\mu}\xi)+\lambda\sqrt{-\mu})$, where $\xi=x+(-3a_0{}^2\alpha-3\alpha\mu^2\lambda^2+\alpha\mu+6\alpha a_0\mu\lambda)\,t$. This has been found as early as 1986 by Hereman et al. [1].

Family 7: $u_{17}(\xi)=a_0+\sqrt{-\mu}(\tanh(A+\sqrt{-\mu}\xi)+\coth(A+\sqrt{-\mu}\xi))$, where $\xi=x+(4\alpha\mu-3a_0{}^2\alpha)\,t$. Obtained before in [11].

Family 8: $u_{18,19}(\xi)=\mp\frac{\sqrt{-\mu}}{3}(\frac{12\mp19\tanh(A+\sqrt{-\mu}\xi)\mp9\coth(A+\sqrt{-\mu}\xi)}{3\mp\tanh(A+\sqrt{-\mu}\xi)}),\ u_{20,21}(\xi)=\mp\frac{\sqrt{-\mu}}{3}(\frac{12\mp19\coth(A+\sqrt{-\mu}\xi)\mp9\tanh(A+\sqrt{-\mu}\xi)}{3\mp\coth(A+\sqrt{-\mu}\xi)})$, where $\xi=x+\frac{28}{3}\alpha\mu\,t$. Family 8 is published in [42].

Family 9: $u_{22}(\xi)=2\sqrt{-\mu}\coth(A+\sqrt{-\mu}\xi),\ u_{23}(\xi)=2\sqrt{-\mu}\tanh(A+\sqrt{-\mu}\xi)$, where $\xi=x+4\alpha\mu\,t$. Family 9 is obtained in [35].

Family 10: $u_{24}(\xi)=2\sqrt{-\mu}(\tanh(A+\sqrt{-\mu}\xi)+\coth(A+\sqrt{-\mu}\xi))$, where $\xi=x+16\alpha\mu\,t$. Family 10 is the linear combination of Family 9.

Family 11: $u_{25,26}(\xi)=\mp\frac{2}{3}\sqrt{-\mu}(\frac{3\mp4\tanh(A+\sqrt{-\mu}\xi)\mp9\coth(A+\sqrt{-\mu}\xi)}{3\mp\tanh(A+\sqrt{-\mu}\xi)}),\ u_{27,28}(\xi)=\mp\frac{2}{3}\sqrt{-\mu}(\frac{3\mp4\coth(A+\sqrt{-\mu}\xi)\mp9\tanh(A+\sqrt{-\mu}\xi)}{3\mp\coth(A+\sqrt{-\mu}\xi)})$, where $\xi=x+\frac{28}{3}\alpha\mu\,t$.

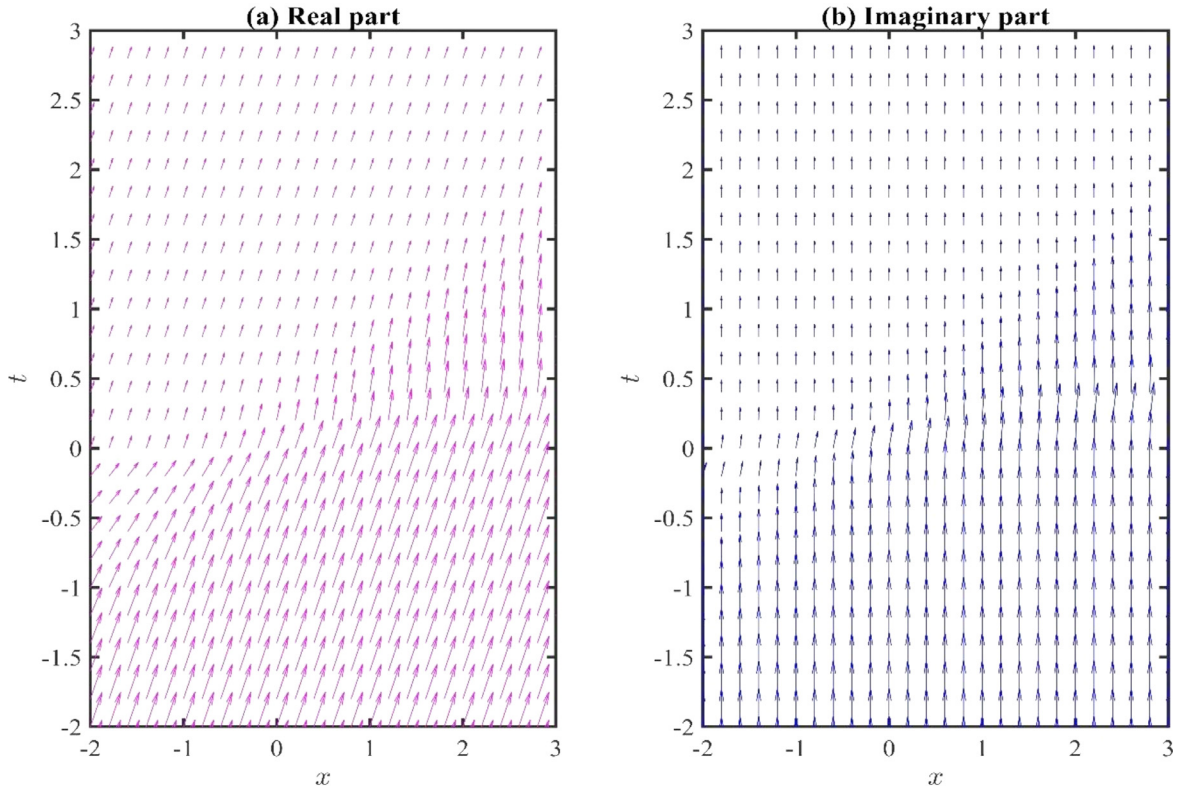

Fig. 10. Instantaneous streamline pattern between $u_1(x,t)$ and $u_{16}(x,t)$ for the values of $\mu=-1,\ A=0,\ a_0=1,\ \alpha=2,\ \lambda=1$. Arrows in figures (a) and (b) depicted the direction of wave components. In Figure (a) real part and Figure (b) imaginary part of $u_1(x,t)$ are used.

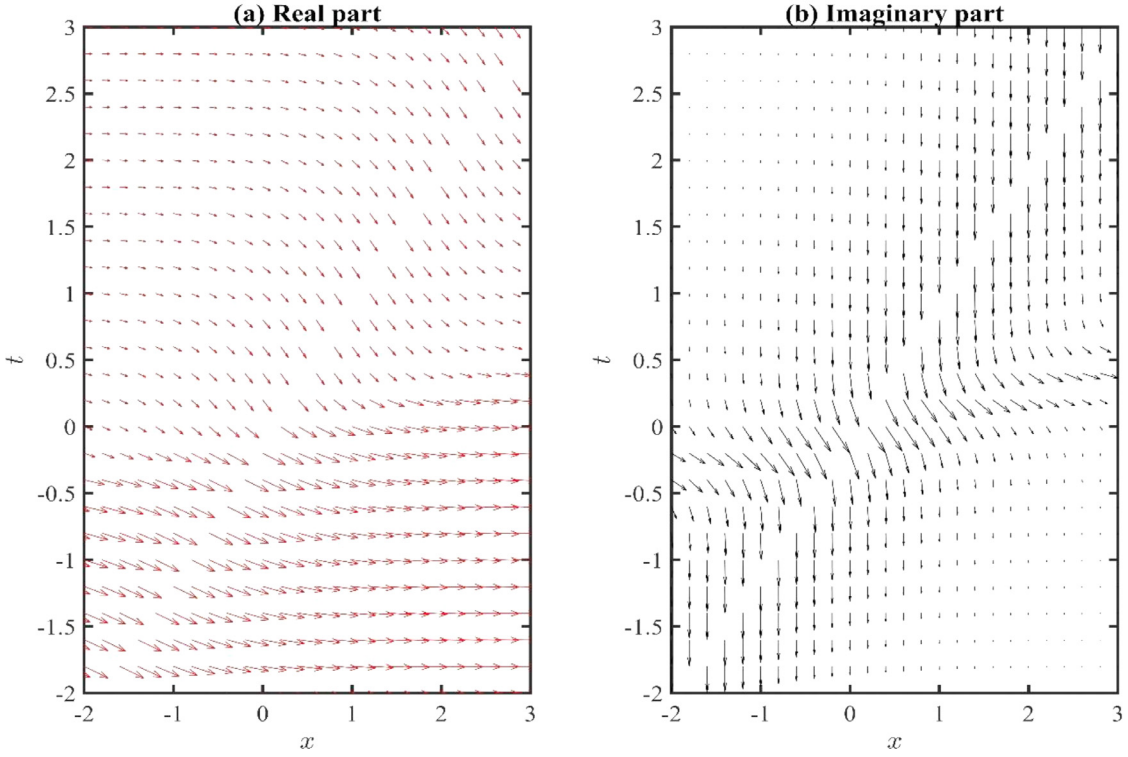

Fig. 11. Instantaneous streamline pattern between $u_1(x,t)$ and $u_{33}(x,t)$ for the values of $\mu=-1,\ A=0,\ a_0=1,\ \alpha=2,\ \lambda=1$. Arrows in figures (a) and (b) depicted the direction of wave components. In Figure (a) real part and Figure (b) imaginary part of $u_1(x,t)$ are used.

Family 12: $u_{29,30}(\xi)=\sqrt{-\mu}(\coth(A+\sqrt{-\mu}\xi)\mp\operatorname{csch}(A+\sqrt{-\mu}\xi))$, $u_{31,32}(\xi)=\sqrt{-\mu}(\tanh(A+\sqrt{-\mu}\xi)\mp I\operatorname{sech}(A+\sqrt{-\mu}\xi))$, where $\xi=x+\alpha\mu t$. (Family 2 and 12 are same)

Family 13: $u_{33,34}(\xi)=\frac{1}{2}\sqrt{-\mu}(\frac{\tanh(A+\sqrt{-\mu}\xi)\pm\coth(A+\sqrt{-\mu}\xi)}{\mp\operatorname{csch}(A+\sqrt{-\mu}\xi)\pm I\operatorname{sech}(A+\sqrt{-\mu}\xi)})$, $u_{35,36}(\xi)=\frac{1}{2}\sqrt{-\mu}(\frac{\coth(A+\sqrt{-\mu}\xi)\pm\tanh(A+\sqrt{-\mu}\xi)}{\mp I\operatorname{csch}(A+\sqrt{-\mu}\xi)\mp\operatorname{sech}(A+\sqrt{-\mu}\xi)})$, where $\xi=x+\alpha\mu t$.

Family 14: $u_{37,38}(\xi)=a_0+\frac{1}{2}\sqrt{-\mu}(\coth(A+\sqrt{-\mu}\xi)\mp\operatorname{csch}(A+\sqrt{-\mu}\xi)+\lambda\sqrt{-\mu})$, $u_{39,40}(\xi)=a_0+\frac{1}{2}\sqrt{-\mu}(\tanh(A+\sqrt{-\mu}\xi)\mp I\operatorname{sech}(A+\sqrt{-\mu}\xi)+\lambda\sqrt{-\mu})$, where $\xi=x+(-\frac{1}{4}\alpha(-\mu-12a_0\mu\lambda+12{a_0}^2+3\mu^2\lambda^2))t$.

Trigonometric function solutions ($\mu>0$): Substituting Eqs. (2.9) and (2.10) into Eq. (3.4) along with Sets 1 - 14, we get the following trigonometric function solutions.

Family 15: $u_{41,42}(\xi)=a_0+\frac{1}{2}\sqrt{\mu}(\tan(A-\sqrt{\mu}\,\xi)\pm\sec(A-\sqrt{\mu}\,\xi))$, $u_{43,44}(\xi)=a_0+\frac{1}{2}\sqrt{\mu}(\cot(A+\sqrt{\mu}\,\xi)\mp\csc(A+\sqrt{\mu}\,\xi))$, where $\xi=x+(\frac{1}{2}\alpha(\mu-12{a_0}^2))t$.

Family 16: $u_{45,46}(\xi)=\sqrt{\mu}(\tan(A-\sqrt{\mu}\xi)\pm\sec(A-\sqrt{\mu}\xi))$, $u_{47,48}(\xi)=\sqrt{\mu}(\cot(A+\sqrt{\mu}\xi)\mp\csc(A+\sqrt{\mu}\xi))$, where $\xi=x+\alpha\mu t$.

Family 17: $u_{49}(\xi)=a_0+\sqrt{\mu}\,(1+\mu\,\lambda^2)(\frac{\tan(A-\sqrt{\mu}\xi)}{1+\lambda\sqrt{\mu}\tan(A-\sqrt{\mu}\xi)})$, $u_{50}(\xi)=a_0+\sqrt{\mu}\,(1+\mu\,\lambda^2)(\frac{\cot(A+\sqrt{\mu}\xi)}{1+\lambda\sqrt{\mu}\cot(A+\sqrt{\mu}\xi)})$, where $\xi=x+(-3{a_0}^2\alpha-3\alpha\mu^2\lambda^2+\alpha\mu-6\alpha a_0\mu\lambda)t$.

Family 18: $u_{51}(\xi)=-2\mu\lambda+2\sqrt{\mu}\,(1+\mu\,\lambda^2)(\frac{\tan(A-\sqrt{\mu}\xi)}{1+\lambda\sqrt{\mu}\tan(A-\sqrt{\mu}\xi)})$, $u_{52}(\xi)=-2\mu\lambda+2\sqrt{\mu}\,(1+\mu\,\lambda^2)(\frac{\cot(A+\sqrt{\mu}\xi)}{1+\lambda\sqrt{\mu}\cot(A+\sqrt{\mu}\xi)})$, where $\xi=x+4\alpha\mu t$.

Family 19: $u_{53}(\xi)=\sqrt{\mu}\,(\frac{(1+\mu\,\lambda^2)\tan(A-\sqrt{\mu}\xi)}{1+\lambda\sqrt{\mu}\tan(A-\sqrt{\mu}\xi)}-\cot(A-\sqrt{\mu}\xi)-\lambda\sqrt{\mu})$,

$u_{54}(\xi)=\sqrt{\mu}\,(\frac{(1+\mu\,\lambda^2)\cot(A+\sqrt{\mu}\xi)}{1+\lambda\sqrt{\mu}\cot(A+\sqrt{\mu}\xi)}-\tan(A+\sqrt{\mu}\xi)-\lambda\sqrt{\mu})$, where$\xi=x+4\alpha\mu t$.

Family 20: $u_{55}(\xi)=a_0-\sqrt{\mu}(\cot(A-\sqrt{\mu}\xi)+\lambda\sqrt{\mu})$, $u_{56}(\xi)=a_0-\sqrt{\mu}(\tan(A+\sqrt{\mu}\xi)+\lambda\sqrt{\mu})$, where $\xi=x+(-3{a_0}^2\alpha-3\alpha\mu^2\lambda^2+\alpha\mu+6\alpha a_0\mu\lambda)t$. Obtained in [35].

Family 21: $u_{57}(\xi)=a_0+\sqrt{\mu}(\tan(A-\sqrt{\mu}\xi)-\cot(A-\sqrt{\mu}\xi))$, $u_{58}(\xi)=a_0+\sqrt{\mu}(\cot(A+\sqrt{\mu}\xi)-\tan(A+\sqrt{\mu}\xi))$, where $\xi=x+(4\alpha\mu-3{a_0}^2\alpha)t$. Obtained in [36].

Family 22: $u_{59,60}(\xi)=\pm\frac{1}{3}I\sqrt{\mu}(\frac{12\mp19I\tan(A-\sqrt{\mu}\xi)\pm9I\cot(A-\sqrt{\mu}\xi)}{3\mp I\tan(A-\sqrt{\mu}\xi)})$, $u_{61,62}(\xi)=\pm\frac{1}{3}I\sqrt{\mu}(\frac{12\mp19I\cot(A+\sqrt{\mu}\xi)\pm9\tan(A+\sqrt{\mu}\xi)}{3\mp I\cot(A+\sqrt{\mu}\xi)})$, where $\xi=x+\frac{28}{3}\alpha\mu t$.

Family 23: $u_{63}(\xi)=-2\sqrt{\mu}\cot(A-\sqrt{\mu}\xi)$, $u_{64}(\xi)=-2\sqrt{\mu}\tan(A+\sqrt{\mu}\xi)$, where $\xi=x+4\alpha\mu t$.

Family 24: $u_{65}(\xi)=2\sqrt{\mu}(\tan(A-\sqrt{\mu}\xi)-\cot(A-\sqrt{\mu}\xi))$, $u_{66}(\xi)=2\sqrt{\mu}(\cot(A+\sqrt{\mu}\xi)-\tan(A+\sqrt{\mu}\xi))$, where $\xi=x+16\alpha\mu t$.

Family 25: $u_{67,68}(\xi)=\pm\frac{2}{3}\sqrt{\mu}(\frac{3\mp4\tan(A-\sqrt{\mu}\xi)\pm9\cot(A-\sqrt{\mu}\xi)}{3\mp\tan(A-\sqrt{\mu}\xi)})$, $u_{69,70}(\xi)=\pm\frac{2}{3}\sqrt{\mu}(\frac{3\mp4\cot(A+\sqrt{\mu}\xi)\pm9\tan(A+\sqrt{\mu}\xi)}{3\mp\cot(A+\sqrt{\mu}\xi)})$, where $\xi=x+\frac{28}{3}\alpha\mu t$.

Family 26: $u_{71,72}(\xi)=-\sqrt{\mu}(\cot(A-\sqrt{\mu}\xi)\mp\csc(A-\sqrt{\mu}\xi))$, $u_{73,74}(\xi)=-\sqrt{\mu}(\tan(A+\sqrt{\mu}\xi)\mp\sec(A+\sqrt{\mu}\xi))$, where $\xi=x+\alpha\mu t$.

Family 27: $u_{75,76}(\xi)=\frac{1}{2}\sqrt{\mu}(\frac{\tan(A-\sqrt{\mu}\xi)-\cot(A-\sqrt{\mu}\xi)}{\mp\csc(A-\sqrt{\mu}\xi)\mp\sec(A-\sqrt{\mu}\xi)})$, $u_{77,78}(\xi)=\frac{1}{2}\sqrt{\mu}(\frac{\cot(A+\sqrt{\mu}\xi)-\tan(A+\sqrt{\mu}\xi)}{\mp\csc(A+\sqrt{\mu}\xi)\mp\sec(A+\sqrt{\mu}\xi)})$, where $\xi=x+\alpha\mu t$.

Family 28: $u_{79,80}(\xi)=a_0-\frac{1}{2}\sqrt{\mu}(\cot(A-\sqrt{\mu}\xi)\mp\csc(A-\sqrt{\mu}\xi)+\lambda\sqrt{\mu})$, $u_{81,82}(\xi)=a_0-\frac{1}{2}\sqrt{\mu}(\tan(A+\sqrt{\mu}\xi)\mp\sec(A+\sqrt{\mu}\xi)+\lambda\sqrt{\mu})$, where $\xi=x+(-\frac{1}{4}\alpha(-\mu-12a_0\mu\lambda+12{a_0}^2+3\mu^2\lambda^2))t$.

4. Analysis of the results

From the obtained fourteen hyperbolic families of STO solutions, one is dependent and six have been published before. About the obtained solutions of the STO equation, it is interesting to point out irregular behavior: solitons emerge from a delicate balance between nonlinear- and linear effects, with full mutual interaction. Solitons reappear after collision by retaining their identities with the same speed and shape. If two solitons collide, they just pass through each other and emerge unchanged thereafter.

4.1. Phenomena of solitons based on the values of the parameters

Below we omit phenomena of solitons' fission and fusion.

For $\mu<0$, Family 1 - 14 are exact solitary wave solutions.

- Family 3: For $-1<\lambda<1$ provides a kink wave; for $\lambda=\pm1$, $\mu=-1$ Family 3 provides trivial solution and for $\lambda<-1$ or $\lambda>1$. Family 3 provides a singular kink wave.
- For $-1<\lambda<1$, Family 3($u_9(\xi)$) and Family 4($u_{11}(\xi)$) are a kink wave and Family 3($u_{10}(\xi)$) and Family 4 ($u_{12}(\xi)$) are singular kink waves.
- For $\lambda=\pm1$, $\mu=-1$ Family 3 and Family 4 give absurd solutions and for $\lambda<-1$ or $\lambda>1$ Family 3 and Family 4 are singular kink waves.
- Family 5: For $\lambda=\pm1$, $\mu=-1$, $u_{13}(\xi)$ is a singular kink solution and $u_{14}(\xi)$ is a kink solution.
- Family 6: For any real value of the parameters, $u_{15}(\xi)$ is a singular kink solution and $u_{16}(\xi)$ is a kink solution.
- Family 9: For any real value of the parameters, $u_{22}(\xi)$ a singular kink solution and $u_{23}(\xi)$ is a kink solution.
- Analogously, Family 1, Family 2, Family 7, Family 8 and Family 10 - 14 represent different solitons for the different real values of the parameters.

Consequently, for $\mu>0$, Families 15 - 28 are trigonometric function solutions, also named plane periodic travelling wave solutions. The phase speed ω plays an important role in the physical structure of the solutions obtained above. For positive values of phase speed ω the disturbances represented by $u(\xi)=u(x+\omega t)$ are moving in the negative x-direction. Consequently, for negative values of the phase speed ω the disturbance move in the positive $x$direction.

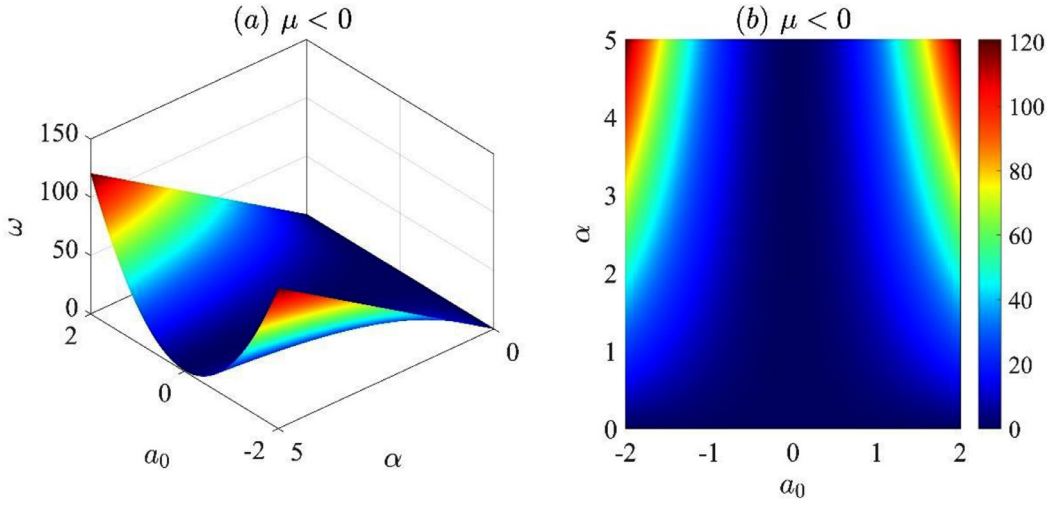

Fig. 12. Phase speed $\omega_1 = \frac{1}{2}\alpha(\mu - 12a_0^2)$ for the phase / travelling wave variable $\xi_1(x,t) = x + \frac{1}{2}\alpha(\mu - 12a_0^2)t$ in Family 1/Family 15 by fixing $\mu = -0.25$ and varying the parameters $a_0 \in [-2,\ 2]$ and $\alpha \in [0,\ 5]$. Figure (a) shows the 3D view whereas Figure (b) represents the corresponding 2D view of the phase speed.

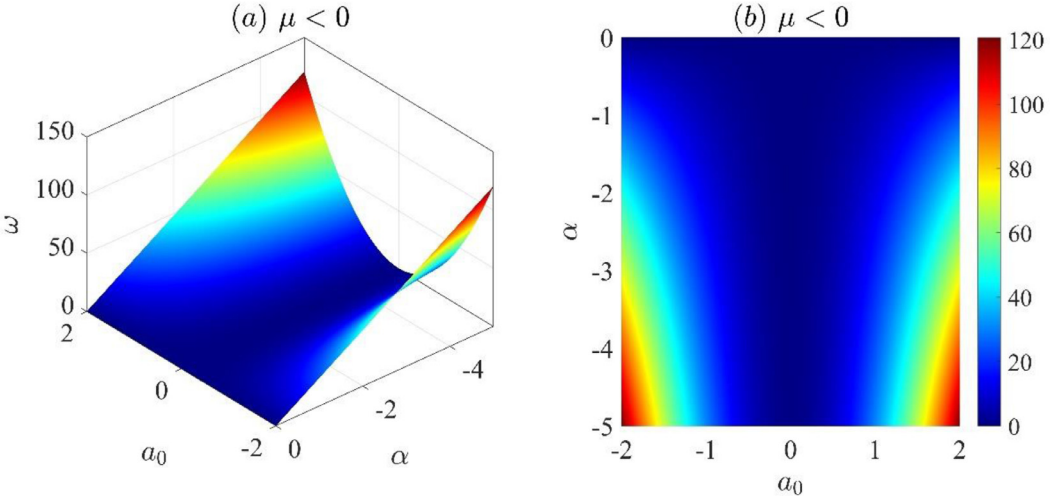

Fig. 13. Phase speed $\omega_1 = \frac{1}{2}\alpha(\mu - 12a_0^2)$ for the phase/ travelling wave variable $\xi_1(x,t) = x + \frac{1}{2}\alpha(\mu - 12a_0^2)t$ in Family 1/Family 15 by fixing $\mu = -0.25$ and varying the parameters $a_0 \in [-2,\ 2]$ and $\alpha \in [-5,\ 0]$. Figure (a) shows the 3D view whereas Figure (b) represents the corresponding 2D view of the phase speed.

4.2. Analysis of the physical structure of the results

In this subsection, we have illustrated the graphical representation of the physical structure and time evolution of some of the obtained solutions of the STO equation in Figs. 1-8.

5. Streamline among the obtained solutions

Now we stress our attention to exploring the instantaneous streamline pattern among the obtained solutions. Simulations are run to explore the local direction of the components of the obtained solitary wave solutions at each point in the coordinate (x,t). We depict instantaneous streamline patterns between some pairs of the obtained solutions in Figs. 9-11.

6. Numerical analysis to examine the influence of the parameters

By setting particular values of the parameters, we can explore the physical structure of phase speed and the phase of the propagating wave as shown in Section 4. Now we stress our attention to analyze, how the phase speed is influenced by the parameters. A sample of simulation results for phase speed is presented in Figs. 12-18.

A numerical sample for phase speed in Family 1: Phase speed in Family 1 is a quadratic function in a_0 obtained as $\omega_{Family_1} = \frac{1}{2}\alpha(\mu - 12a_0^2)$. In this sample, we have taken $\mu = -0.25$. In this sample, we have taken μ constant and very through a_0 and . Fixing $\mu = -0.25$ we checked the profile of phase speed of Family 1 for a sequence of values of a_0 and α; the results are illustrated in Fig. 12 and Fig. 13. Numerical simulations in Fig. 12 indicates that-

(a) for $a_0 \to \pm\infty,\ \alpha \to \infty$, the phase speed $\omega \to \infty$; that is phase speed increases
(b) for $a_0 \to \pm\infty, \alpha \to 0$, the phase speed $\omega \to 0$; that is phase speed decreases
(c) for $a_0 \to 0,\ \alpha \to [0,\ \infty]$, the phase speed $\omega \to 0$; that is phase speed decreases

Numerical simulations in Fig. 13 indicates that-

(a) for $a_0 \to \pm\infty,\ \alpha \to -\infty$, the phase speed $\omega \to \infty$; that is phase speed increases
(b) for $a_0 \to \pm\infty, \alpha \to 0$, the phase speed $\omega \to 0$; that is phase speed decreases

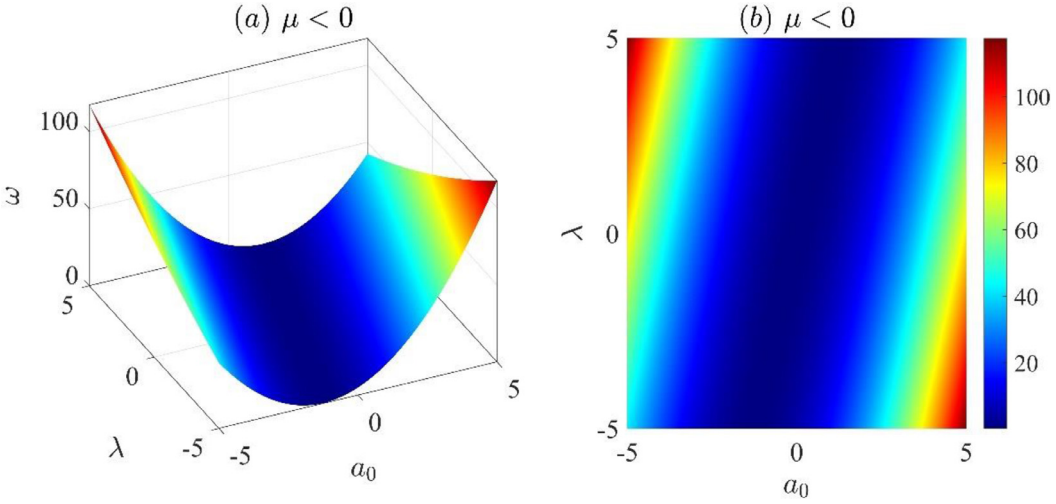

Fig. 14. Effect of the parameters on phase speed of Family 3: fixing $\alpha = 1,\ \mu = -0.25$ we checked the profile of phase speed for a sequence of values of $[a_0,\ \lambda] \in [-5,\ 5]$. Figure (a) shows the 3D view whereas Figure (b) represents the corresponding 2D view of the phase speed.

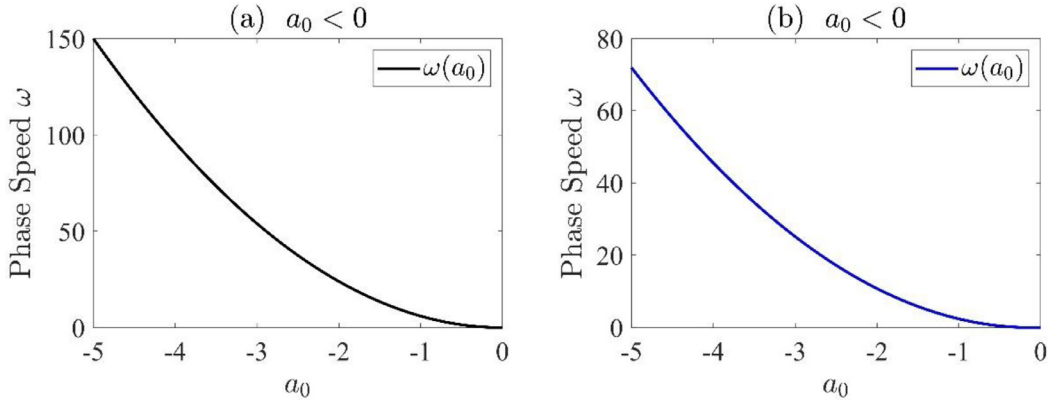

Fig. 15. Phase speed profiles for the fixed values of $\lambda = 1,\ \mu = 0.1,\ \alpha = 1$ by varying the parameter a_0. Figure (a) corresponds to the phase speed in Family 1 and Figure (b) is the corresponding phase speed in Families 3, 6. Figure (a) and Figure (b) show quadratic growth in a_0 in the form $\omega \to 0$ as $a_0 \to 0$ and $\omega \to \infty$ as $a_0 \to -\infty$.

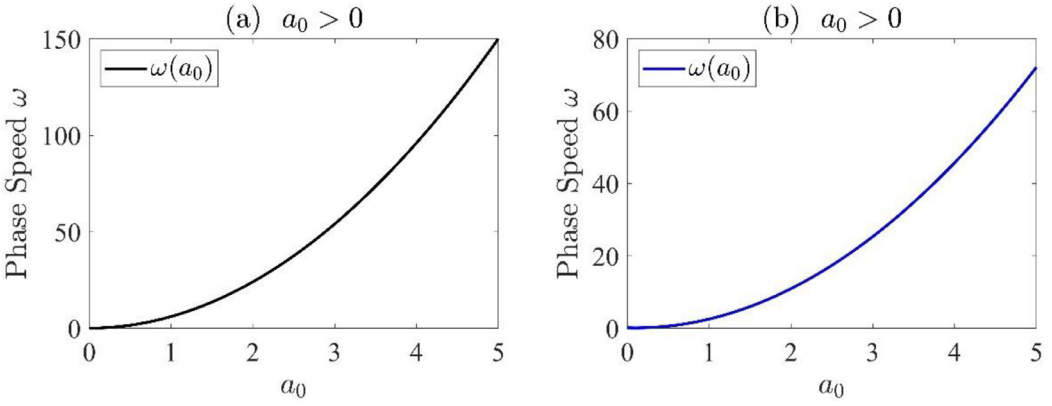

Fig. 16. Phase speed profiles for the fixed values of $\lambda = 1,\ \mu = 0.1,\ \alpha = 1$ by varying the parameter a_0. Figure (a) corresponds to the phase speed in Family 15 and Figure (b) is the corresponding phase speed in Families 17, 20. Figure (a) and Figure (b) show quadratic growth in a_0 in the form $\omega \to 0$ as $a_0 \to 0$ and $\omega \to \infty$ as $a_0 \to \infty$.

(c) for $a_0 \to 0,\ \alpha \to [-\infty,\ 0]$, the phase speed $\omega \to 0$; that is phase speed decreases

A numerical sample for phase speed in Family 3: Phase speed in Family 3 is a quadratic function in $a_0,\ \mu$ and λ defined by $\omega_{Family_3} = -\alpha(3\mu^2\lambda^2 + 3a_0^2 - \mu + 6a_0\mu\lambda)$. In this sample, we have taken $\alpha,\ \mu$ constants and very through a_0 and . Fixing $\alpha = 1,\ \mu = -0.25$ we checked the profile of phase speed of Family 3 for a sequence of values of a_0 and λ in the interval $[-5,\ 5]$; the result is illustrated in Fig. 14, which indicates that –

(a) for $a_0 \to \infty,\ \lambda \to -\infty$ phase speed $\omega \to \infty$; that is phase speed increases
(b) for $a_0 \to -\infty,\ \lambda \to \infty$ phase speed $\omega \to \infty$; that is phase speed increases with the increase of the parameters a_0 and λ with opposite signs.

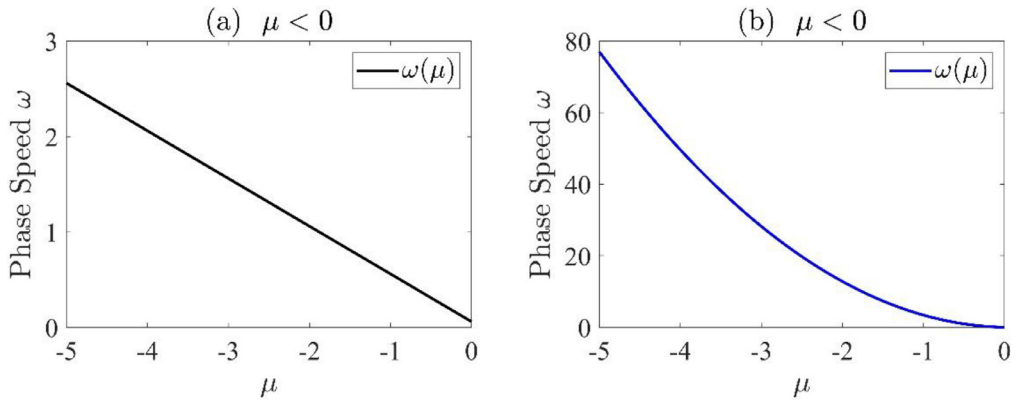

Fig. 17. Phase speed profiles: Figure (a) corresponds to the phase speed in Family 1 and Figure (b) is the corresponding phase speed in Families 3, 6. Figure (a) is the behavior of phase speed (black curve) showing linear growth in μ in the form $\omega \to 0$ as $\mu \to 0$ and $\omega \to \infty$ as $\mu \to -\infty$. Whereas Figure (b) is the behavior of phase speed showing quadratic growth in μ in the form $\omega \to 0$ as $\mu \to 0$ and $\omega \to \infty$ as $\mu \to -\infty$.

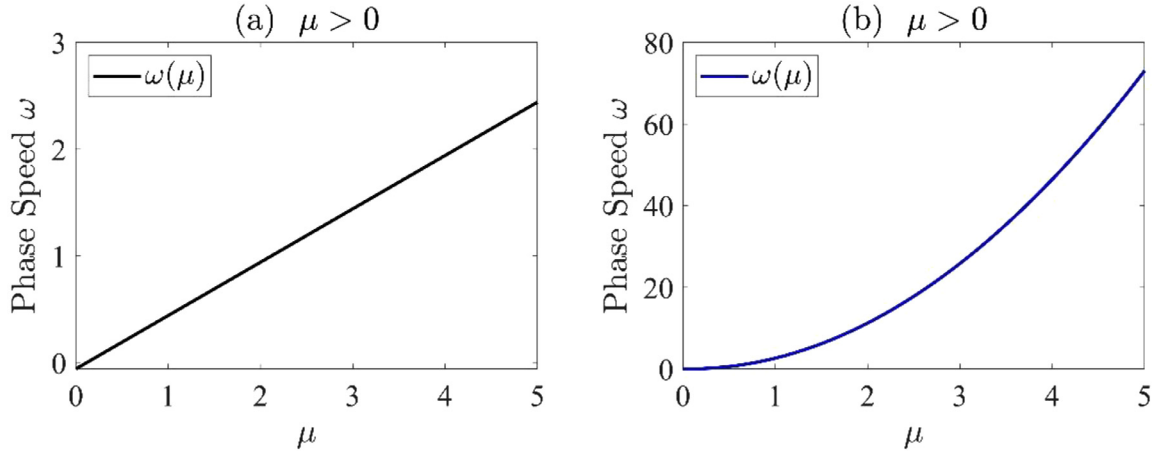

Fig. 18. Phase speed profiles. Figure (a) corresponds to the phase speed in Family 15 and Figure (b) is the corresponding phase speed in Families 17, 20. Figure (a) is the behavior of phase speed (black curve) showing linear growth in μ in the form $\omega \to 0$ as $\mu \to 0$ and $\omega \to \infty$ as $\mu \to \infty$. Whereas Figure (b) is the behavior of phase speed showing quadratic growth in μ in the form $\omega \to 0$ as $\mu \to 0$ and $\omega \to \infty$ as $\mu \to \infty$.

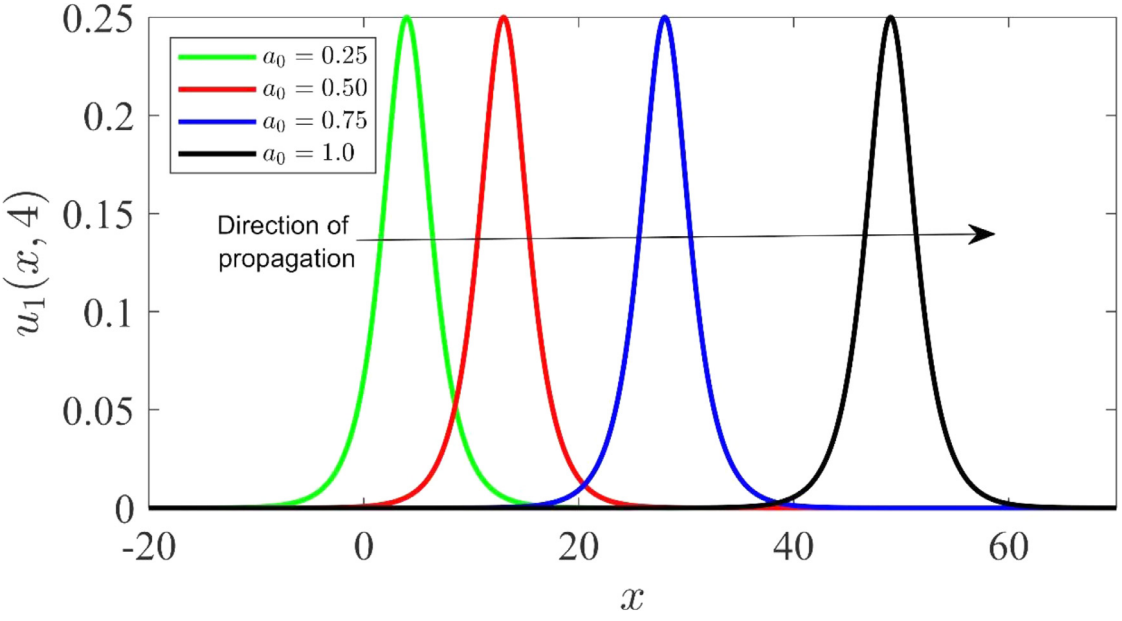

Fig. 19. Graphs of solitary wave profile u_1 influenced by the parameter a_0 when propagating along the x-axis. Snapshots for different values of a_0 with the values of $\mu = -0.25$, $A = 0$, $\alpha = 2$ are taken at time $t = 4$. This figure indicates that with the increase of the value of the parameter a_0, keeping the values of other parameters fixed, solitons can travel faster.

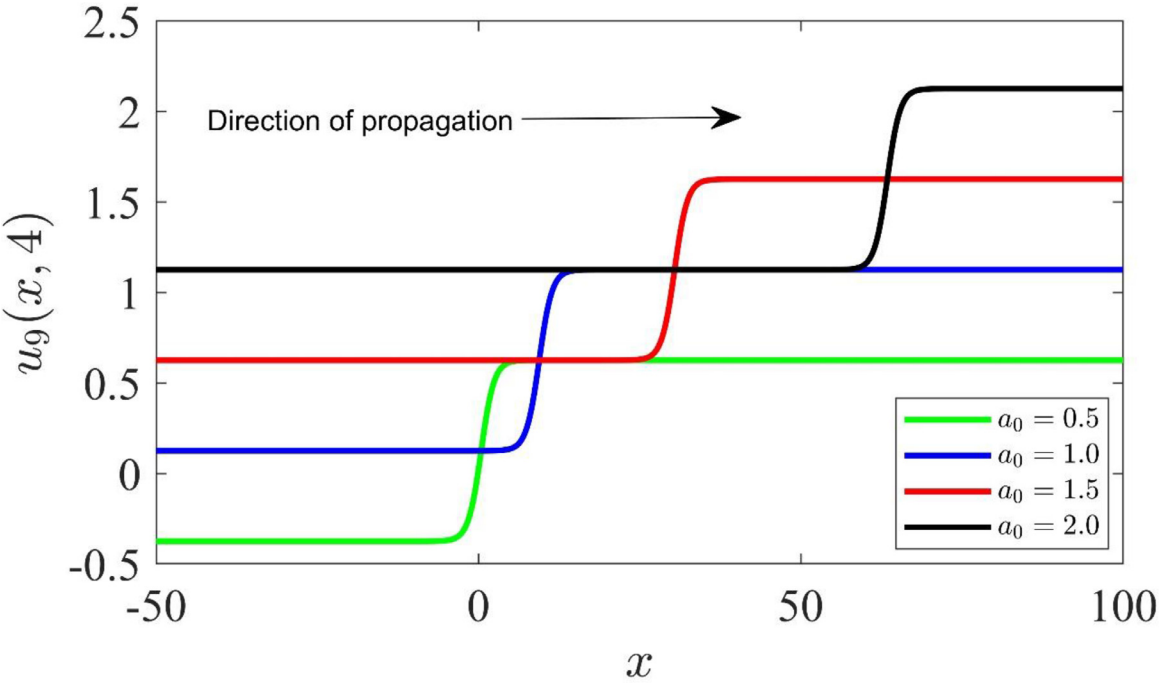

Fig. 20. Graphs of solitary wave profile u_9 influenced by the parameter a_0 when propagating along the x-axis. Snapshots for different values of a_0 with the values of $\mu = -0.25$, $A = 0$, $\alpha = 2$, $\lambda = 1.5$ are taken at time $t = 4$. This figure indicates that with the increase of the value of the parameter a_0, keeping the values of other parameters fixed, solitons can travel faster.

(c) for $a_0 \to 0$, $\lambda \to [-\infty, +\infty]$ phase speed $\omega \to 0$; that is phase speed decreases

In Figs. 15-18 effect of single parameters on phase speed are depicted. Analogously we can explain the phase speed for other families. Note that we only took for the magnitude of the phase speed to determine the impact of parameters on it.

The above phase speed analysis indicates that the parameters play an important role in the travelling wave phenomena as the change of the values of the parameters alter the phase speed. We now attempt to formalize the numerical results by changing the variables, to analyze the impact of the variables, on the travelling wave solutions of the STO equations. Sample simulated results are illustrated in Figs. 19 and 20 to understand the influence of the parameters in the obtained solutions. Figs. 19 and 20, indicate that with the increase of the parameter a_0 the *solitary waves can travel faster*. Overall, the results in Figs. 12-20 reveal a novel application of the parameters to get the expected pattern of the travelling periodic or solitary waves with the required phase speed for a certain field of research.

Analogously we can explore the impact of the other parameters in the obtained solutions.

Analysis of the STO model, for $a_0 \to \infty$, indicates that the phase speed associated with travelling wave solutions of the STO model travels faster. This observation is mathematically interesting because best of our knowledge in the previous study of the STO model the impact of phase speed analysis is ignored.

7. Conclusions

In this work, we study travelling wave solutions of the STO equation. The enhanced (G'/G)-expansion method has been applied successfully and then several numerical simulations are run to analyze our results. Instantaneous streamline patterns among some randomly selected solitary wave solutions are depicted successfully through numerical simulations, to explore the local direction of the components of the obtained solitary wave solutions at each point in the coordinate (x, t). Numerical simulations of the obtained solutions show that there is a complicated relationship between the phase speed of the travelling wave solutions and the parameters in the solutions. It is because the phase speed in terms of the parameters is not unified. Our numerical analysis suggests that the phase speed is proportional to the parameters (or proportional to the square of the parameters). Overall, our analysis and numerical exploration show that there are numerous opportunities to extend the work presented in this study. The more arbitrary parameters in the obtained solutions imply that solutions have richer local structures. It is illustrated that the enhanced (G'/G)-expansion method is direct, and effectively can be used for many other applications of nonlinear evolution equations (NLEEs) to play an important role in the understanding of qualitative features of phenomena and processes modelled, for example in physics, chemistry [37], biology [38,39] and (nanotechnology-)engineering [40,41,42]. Exact solutions specifically exemplify graphically complex nonlinear properties of such models, to disentangle mechanisms such as spatial localization of transfer processes, multiplicity or absence, of steady states, the existence of peaking regimes, etc. Even without application persé may exact solutions play a rôle as test problems to verify consistency and estimate errors of numerical, asymptotic, or approximate analytical 'theoretical' methods. In this way can exact solutions serve as a basis for perfecting and testing computer algebra software packages (for solving NLEEs).

Declaration of Competing Interest

The authors declare that they have no known competing financial interests or personal relationships that could have appeared to influence the work reported in this paper.

References

[1] W. Hereman, P.P. Banerjee, A. Korpel, et al., J. Phys. A. Math. Gen. 19 (1986) 607–628.
[2] A. Chen, Phys. Lett. Sect. A Gen. At. Solid State Phys. [Internet]. 374 (2010) 2340–2345.

[3] Y. Shang, Y. Huang, W. Yuan, Appl. Math. Comput. 217 (2011) 7172–7183.
[4] A.-.M. Wazwaz, Rom. Rep. Phys. 65 (2013) 383–390.
[5] Y. Zhou, F. Yang, Q Liu, Commun. Nonlinear Sci. Numer. Simul. [Internet]. 16 (2011) 641–646.
[6] S. Wang, X.Y. Tang, S.Y. Lou, Chaos Solitons Fractals 21 (2004) 231–239.
[7] G. Wang, A.H. Kara, Chaos, Solitons Fractals [Internet]. 81 (2015) 290–298.
[8] A. Ghafoor, S. Firdous, T. Zubair, et al., QScience Connect 24 (2013) 1–12.
[9] V.V. Gudkov, J. Math. Phys. 38 (1997) 4794–4803.
[10] A. Bekir, A. Boz, Phys. Lett. A [Internet]. 372 (2008) 1619–1625.
[11] Y. He, S. Li, Y Long, J. Appl. Math. 2013 (2013) 1–6.
[12] A.-.M. Wazwaz, Appl. Math. Comput. 188 (2007) 1205–1213.
[13] K. Khan, M.A. Akbar, J. Egypt. Math. Soc. [Internet]. 22 (2014) 220–226 Available from http://www.sciencedirect.com/science/article/pii/S1110256X13000990 .
[14] M.E. Islam, K. Khan, M.A. Akbar, et al., Int. J. Partial Differ. Eqs. Appl. 1 (2013) 6–12.
[15] K. Khan, M.A. Akbar, M.M. Rashidi, et al., Waves in Random Complex Media [Internet] 25 (2015) 644–655 Available from: http://www.tandfonline.com/doi/full/10.1080/17455030.2015.1068964 .
[16] K. Khan, M.A.A. Akbar, H. Koppelaar, R. Soc. Open Sci. 2 (2015) 1–13.
[17] H. Naher, F.A. Abdullah, J. Egypt. Math. Soc. [Internet]. 22 (2014) 390–395 Available from: http://dx.doi.org/, doi:10.1016/j.joems.2013.11.008.
[18] N.A. Kudryashov, Commun. Nonlinear Sci. Numer. Simul. [Internet]. 14 (2009) 3507–3529 Available from: http://dx.doi.org/, doi:10.1016/j.cnsns.2009.01.023.
[19] A.S. Sharma, H. Tasso, Connection Between Wave Envelope and Explicit Solution of a Nonlinear Dispersive Wave Equation, Muenchen, Germany, 1977.
[20] P.J. Olver, J. Math. Phys. 18 (1977) 1212–1215.
[21] F. Verheest, W. Hereman, J. Phys. A. 15 (1982) 95–102.
[22] A.-.M.M. Wazwaz, S.A. El-Tantawy, Nonlinear Dyn. 87 (2016) 2457–2461.
[23] S. Bibi, S.T. Mohyud-Din, R. Ullah, et al., Results Phys. [Internet]. 7 (2017) 4434–4439 Available from:, doi:10.1016/j.rinp.2017.11.009.
[24] E Fan, J. Math. Phys. 42 (2001) 4327–4344.
[25] E Fan, Phys. A [Internet] 301 (2001) 105–113 Available from www.elsevier.com/locate/physa .
[26] Y.C. Hon, E Fan, Chaos, Soliton Fractals [Internet]. 24 (2005) 1087–1096 Available from www.elsevier.com/locate/chaos .
[27] H. Zhao, Chaos An Interdiscip. J. Nonlinear Sci. [Internet] 27 (2017) 1–7.
[28] N.A. Kudryashov, Prikl. Matem. Mokhan. U.S.S.R [Internet] 52 (1988) 361–365 [cited 2017 Oct 24]Available from: http://www.sciencedirect.com/science/article/pii/0021892888900901 .
[29] A. Kirsch, An Introduction to the Mathematical Theory of Inverse Problems [Internet], Springer, 2011 Available from: file:///Users/Brian_Caudle/Documents/Papers/2004/Marsen/Applied Mathematical Sciences 2004 Marsen.pdf%5Cnpapers://75088281-f09c-4e77-b8c2-14041f4545f6/Paper/p785%5Cnhttp://books.google.com/books?hl=en&lr=&id=RTo9ZFaSSugC&pgis=1.
[30] I.E. Inan, Y. Uğurlu, H. Bulut, Optik (Stuttg) 127 (2016) 10780–10785.
[31] A.H. Salas, Appl. Math. Sci. 5 (2011) 2289–2295.
[32] L. Song, Q. Wang, H. Zhang, J. Comput. Appl. Math. [Internet] 224 (2009) 210–218.
[33] Y. Zhang, IAENG J. Appl. Math. 46 (2016) 383–388.
[34] B. Erbaş, E. Yusufoğlu, Chaos Solitons Fractals. 41 (2009) 2326–2330.
[35] A.J.M. Jawad, M.D. Petkovic, A. Biswas, Appl. Math. Comput. 217 (2010) 869–877.
[36] M. Tolbert, Acc. Chem. Res. 25 (1992) 561–568.
[37] EV Nikolova, IP Jordanov, ZI Dimitrova, et al., Appl. Math. Tech. Nat. Sci. AIP Conf. Proc. [Internet]. American Institute of Physics (2017) 070001–070008.
[38] E. Villagran Vargas, A. Ludu, R. Hustert, et al., Biophys. Chem. [Internet]. 153 (2011) 159–167.
[39] E.M.E. Zayed, A.-.G. Al-Nowehy, Indian J. Phys. 91 (2016) 209–218.
[40] M.B. Hubert, G. Betchewe, S.Y. Doka, et al., Appl. Math. Comput. [Internet]. 239 (2014) 299–309.
[41] T.B. Sisan, S. Lichter, Phys. Rev. Lett. 112 (2014) 1–5.
[42] H. Dai, L. Li, Br. J. Math. Comput. Sci. [Internet]. 17 (2016) 1–10.
[43] H.H. Kuehl, C.Y. Zhang, Phys. Fluids B 2 (5) (1990) 889–900.
[44] S. Wang, G. Chen, Nonlinear Anal. 64 (1) (2006) 159–173.
[45] L. Akinyemi, K.S. Nisar, C.A. Saleel, H. Rezazadeh, P. Veeresha, M.M. Khater, M. Inc, Result. Phys. 31 (2021) 104958.
[46] ... & L. Akinyemi, H. Rezazadeh, Q.H. Shi, M. Inc, M.M. Khater, H. Ahmad, M.A. Akbar, Result. Phys. 29 (2021) 104656.
[47] A. Houwe, S. Abbagari, S.Y. Doka, M. Inc, T.B. Bouetou, Chaos Solitons Fractals 151 (2021) 111254.
[48] ... & L. Akinyemi, H. Rezazadeh, S.W. Yao, M.A. Akbar, M.M. Khater, A. Jhangeer, H. Ahmad, Result. Phys. 26 (2021) 104411.
[49] F. Tchier, E.C. Aslan, M. Inc, J. Nanoelectron. Optoelectron. 12 (5) (2017) 526–531.
[50] F. Tchier, A.I. Aliyu, A. Yusuf, M. Inc, Eur. Phys. J. Plus 132 (3) (2017) 1–9.
[51] M.M.A. Khater, A. Jhangeer, H. Rezazadeh, et al., Opt Quant Electron 53 (2021) 609.
[52] F.S. Khodadad, S.M. Mirhosseini-Alizamini, B. Günay, L. Akinyemi, H. Rezazadeh, M. Inc, Opt. Quantum Electron. 53 (12) (2021) 1–17.
[53] Y.Q. Chen, Y.H. Tang, J. Manafian, H. Rezazadeh, M.S. Osman, Nonlinear Dyn. 105 (3) (2021) 2539–2548.
[54] Z. Pinar, H. Rezazadeh, M. Eslami, Opt Quant. Electron. 52 (2020) 504.
[55] W.X. Ma, Int. J. Nonlinear Sci. Numer. Simul. (2021).
[56] W.X. Ma, Symmetry (Basel) 13 (11) (2021) 2205.
[57] W.X. Ma, Partial Differ. Eqs. Appl. Math. 4 (2021) 100190.
[58] W.X. Ma, J. Geom. Phys. 165 (2021) 104191.
[59] W.X. Ma, X. Yong, X. Lü, Wave Motion 103 (2021) 102719.
[60] M.A. Arefin, M.A. Saeed, M.A. Akbar, M.H. Uddin, J. Ocean Eng. Sci. (2021).
[61] A. Ali, A.R. Seadawy, Journal of Ocean Engineering and Science 6 (1) (2021) 85–98.
[62] A.C. Varsoliwala, T.R. Singh, J. Ocean Eng. Sci. 6 (4) (2021) 367–375.
[63] A.A. Gaber, J. Ocean Eng. Sci. 6 (3) (2021) 292–298.
[64] J.R. Holton, Am. J. Phys. 41 (5) (1973) 752–754.
[65] P.H. LeBlond, L.A. Mysak, Waves in the Ocean, Elsevier, 1981.